Soft Matter

ARTICLE TYPE

Cite this: DOI: 00.0000/xxxxxxxxxx

Segregative Phase Separation of Strong Polyelectrolyte Complexes at High Salt and High Polymer Concentrations†

Conner H. Chee, Rotem Benharush, Lexi R. Knight, and Jennifer E. Laaser*

Received Date
Accepted Date

DOI: 00.0000/xxxxxxxxxx

The phase behavior of polyelectrolyte complexes and coacervates (PECs) at low salt concentrations has been well characterized, but their behavior at concentrations well above the binodal is not well understood. Here, we investigate the phase behavior of stoichiometric poly(styrene sulfonate)/poly(diallyldimethylammonium) mixtures at high salt and high polymer concentrations. Samples were prepared by direct mixing of PSS/PDADMA PECs, water, and salt (KBr). Phase separation was observed at salt concentrations approximately 1 M above the binodal. Characterization by thermogravimetric analysis, FTIR, and NMR revealed that both phases contained significant amounts of polymer, and that the polymer-rich phase was enriched in PSS, while the polymer-poor phase was enriched in PDADMA. These results suggest that high salt concentrations drive salting out of the more hydrophobic polyelectrolyte (PSS), consistent with behavior observed in weak polyelectrolyte systems. Interestingly, at the highest salt and polymer concentrations studied, the polymer-rich phase contained both PSS and PDADMA, suggesting that high salt concentrations can drive salting out of partially-neutralized complexes as well. Characterization of the behavior of PECs in the high concentration limit appears to be a fruitful avenue for deepening fundamental understanding of the molecular-scale factors driving phase separation in these systems.

1 Introduction

Polyelectrolyte complexes (PECs) are a class of materials that form when oppositely charged polyelectrolytes are mixed in solution. Under the right solution conditions, such mixtures can undergo associative phase separation to form a polymer rich phase called a polyelectrolyte complex (if the polymer-rich phase is solid or gel-like) or coacervate (if the polymer-rich phase is liquid-like) below a polymer-poor supernatant[1]. The polymer-rich polyelectrolyte complex and coacervate phases have a wide range of applications, including drug delivery[2–5], underwater adhesives[6–8], and salt-processable materials[9–11], to name only a few. These applications are enabled by the specific phase behavior and viscoelasticity of the polymer-rich phase. Thus, developing a comprehensive understanding of the phase behavior in these systems is critical to inform design of functional materials with well-controlled properties.

Over the past few decades, a number of experimental and theoretical efforts have yielded a deep understanding of the phase behavior of PEC systems[1]. Polyelectrolyte complex coacervation is typically observed at low salt and polymer concentrations, where the initial complexation is driven by the entropic gains upon release of counterions from the polyelectrolyte chains and rearrangement of water molecules around the charged species[12–15]. At high salt concentrations, this driving force is reduced, and there is a critical salt concentration above which no phase separation is observed. The phase boundary is typically described by a binodal curve, which separates the 2-phase region at low salt and low polymer fractions from the 1-phase region observed at higher salt concentrations. Binodal curves have been experimentally mapped out for many different polyelectrolyte systems[16–19], and the phase behavior of these systems is found to depend on both the chemical compositions of the polyelectrolytes[17,18,20–22] and solution conditions such as pH[16,23], temperature[24,25], and the identity of the salt used to set the total ionic strength[26,27]. A number of theoretical models have also been developed that successfully describe much of the experimentally-observed phase behavior of these systems. One of the earliest and most widely-used models is the Voorn-Overbeek model, which describes the free energy of mixing in terms of the charge interactions and entropies of different species[28]. Development of both more sophisticated theoretical models and computer simulations that account for chain connectivity, charge sequence, and ion pairing, among other features, have since refined the field's understanding of the

* Department of Chemistry, University of Pittsburgh, 219 Parkman Ave, Pittsburgh, PA, USA. E-mail: j.laaser@pitt.edu

† Electronic Supplementary Information (ESI) available: additional characterization data (TGA, FTIR, and NMR) for reported materials. See DOI: 10.1039/cXsm00000x/

thermodynamics of the complexation process[1,15,29–38].

While a small number of studies have investigated the phase behavior of polyelectrolyte complexes at high polymer concentrations[16,39,40], the vast majority of experimental and theoretical work to date has focused on the low salt and low polymer concentration limits. In practice, most applications of polyelectrolyte complexes and coacervates occur in this limit, and theoretical models have generally predicted that there should be no further phase separation above the binodal. Recently, however, experiments at high salt and high polymer concentrations challenged this assumption. Mixtures of poly(acrylic acid) (PAA) with PDADMA were found to exhibit "re-entrant" phase separation at salt concentrations well above the critical salt concentration[41,42], while mixtures of PAA with poly(allylamine hydrochloride) (PAH) exhibit a continuous two-phase region up to 6 M NaCl[16]. The unexpected observation of phase separation at high salt and at high polymer concentrations suggests that the phase behavior of polyelectrolyte complexes in this regime is more complex than previously understood. Li et al. suggested that these observations could be explained for systems containing PAA by accounting for changes in the polymer-water interaction parameter when PAA is partially protonated below its pKa[42]. Using a thermodynamic model that included a Flory-Huggins interaction parameter describing the non-electrostatic interactions between the polyelectrolytes and solvent, they showed that a second phase separated regime emerged at high salt and high polymer concentrations when the polymer-water interaction parameter was above approximately 0.5. Interestingly, the phase separation at high salt concentrations was predicted to be segregative, with the polyanion and polycation partitioning into different phases, in contrast to the associative phase separation observed at low salt concentrations. While experimental characterization of the separated phases produced at high salt concentrations was limited, the prediction of segregative phase separation was consistent with ^{13}C NMR measurements on a PAA/PDADMA sample prepared at high salt concentration[42], and with both molecular dynamics simulations[43] and the enrichment of PAA in the polymer-rich phase of PAA/PAH and PAA/PDADMA complexes observed in other work[40,41].

Across this work, segregative phase separation at high salt concentrations was predicted to depend strongly on the protonation state of the poly(acrylic acid), with phase separation emerging only once the PAA was partially neutralized and hydrophobic effects began to dominate[42]. Some experiments suggest, however, that a second two-phase window may also emerge at high salt concentrations in complexes of strong polyelectrolytes. In 2020, Morin et al. prepared samples of poly(styrene sulfonate) (PSS) and poly(diallyldimethylammonium) (PDADMA) at salt and polymer concentrations well above the binodal curve, in an effort to decouple salt and polymer-dependent contributions to the materials' dynamics. While all of the samples were expected to be homogeneous, signs of phase separation were observed at salt concentrations above approximately 2 M[44]. This result suggests that the occurrence of a second critical salt concentration above the standard binodal may be a more universal feature of polyelectrolyte complex materials.

Here, we test this hypothesis by preparing stoichiometrically-balanced mixtures of PSS and PDADMA (both strong polyelectrolytes) whose polymer and salt concentrations lie well above the binodal. We find that at salt concentrations up to approximately 1 M above the binodal, the mixtures form a single-phase solution. At higher salt concentrations, however, phase separation is observed. TGA, FTIR, and NMR reveal that the PDADMA and PSS indeed partition to separate phases, although the extent of the PSS/PDADMA partitioning decreases with further increases in the polymer and salt concentrations. These results suggest that segregative phase separation occurs at high salt concentrations even in strong polyelectrolyte systems, and provide evidence for a continuous transition to a third phase-separated regime in which both polyelectrolytes salt out. This work highlights the need to account for non-ionic interactions to fully understand the phase behavior of polyelectrolyte complexes and coacervates, and suggests that further exploration of the high salt regime offers new opportunities to understand the fundamental interactions that drive phase separation in these materials.

2 Experimental Methods

2.1 Materials

Poly(sodium 4-styrene sulfonate) (PSSNa, M_w = ~200,000 g · mol^{-1}, 20 wt%) solution and poly(diallyldimethylammonium chloride) (PDADMAC, M_w = 200,000-350,000 g · mol^{-1}, 23 wt%) solution were purchased from Sigma Aldrich. Potassium bromide (KBr) was purchased from Fisher Scientific. All samples were prepared using Milli-Q water obtained from a Synergy UV water purification system purchased from Millipore Sigma. All materials, except for PSSNa and PDADMAC, were used as received. PSSNa and PDADMAC were dialyzed before use using standard RC dialysis tubing with a molecular weight cutoff of 6-8 kg · mol^{-1} (Spectra/Por, 08-670D).

2.2 Sample Preparation

Samples were prepared by direct mixing of dried PEC, salt, and water, as shown in Fig 1. Briefly, a bulk PEC was first prepared by dissolving stoichiometric amounts of PSSNa and PDADMAC in a 2.5 M KBr solution. Milli-Q water was then added slowly until the KBr concentration was below 0.1 M, resulting in precipitation of the PSS/PDADMA complex. The supernatant was decanted, replaced with milliQ water, and the PEC was allowed to sit for 24 hours to wash out excess salt. This process was repeated a total of three times. The bulk PEC was then dried using a lyophilizer and ground with a mortar and pestle, yielding a white powder. NMR revealed that this parent PEC was stoichiometrically balanced, containing 50.7% PSS and 49.3% PDADMA repeat units (see Electronic Supplementary Information[†]). Samples with targeted PEC and salt concentrations were then prepared by combining the requisite amounts of dry PEC, KBr, and water in an Eppendorf tube. To ensure complete mixing, the samples were vortexed for 1 minute at 2000 rpm after each addition. Samples were then centrifuged for 1 hour at 4000 rpm, left to equilibrate for 2 days, centrifuged again for 1 hour, and left to equilibrate for at least 1 week before characterization.

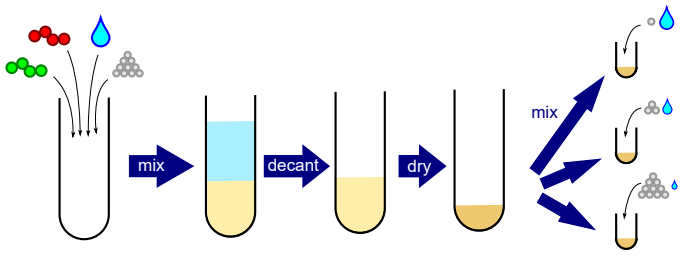

Fig. 1 Schematic of direct addition method used in this work. A bulk PEC was first prepared and dried. Varying amounts of PEC, KBr and water were then mixed to obtain sample compositions above the binodal.

2.3 Thermogravimetric Analysis

Thermogravimetric analysis (TGA) measurements were carried out on a Q5000 IR Thermogravimetric Analyzer (TA Instruments) using a protocol adapted from Li *et al.*[16] For each measurement, approximately 15 mg of sample was loaded onto a platinum pan. The sample was held at 25°C for 5 minutes, and was then heated to 100°C at 20°C · min^{-1} and held at this temperature for 1 hour to drive off water. The temperature was then ramped to 600 °C at a rate of 10 °C · min^{-1} and the sample was held at 600 °C for an additional 1 hour to ensure complete removal of organic components of the sample. The temperature was then finally ramped to 680 °C at 10 °C · min^{-1} to complete the measurement. All measurements were carried under air to facilitate the complete removal of the organic components. Measurements on standard solutions with known compositions indicated that this protocol yielded compositions accurate to within 1 wt%.

2.4 Infrared Spectroscopy

Attenuated Total Reflection-Fourier Transform Infrared Spectroscopy (ATR-FTIR) measurements were carried out on a Spectrum Two (Perkin Elmer) instrument. Measurements were acquired at a resolution of 1 cm^{-1} with a sampling interval of 0.25 cm^{-1} and were averaged over 16 scans. For the polymer rich phases, the sample was compressed with the instrument's pressure gauge until the pressure read 100 Pa to ensure sufficient contact between the polymer sample and the ATR crystal.

2.5 Nuclear Magnetic Resonance

^{1}H-NMR (Avance 400 MHz, Bruker) spectra were used to determine the polymer stoichiometry in each sample. The polymer rich and polymer poor phases of the phase-separated samples were separated and dried with a lyophilizer. The dried samples, which consisted of polymer and salt, were ground with a mortar and pestle, and were then dissolved in a 2.5 M KBr solution in D_2O, targeting a polymer concentration of 15 mg·ml^{-1}. NMR measurements were finally carried out using a relaxation delay (d1 time) of 10 seconds to ensure accurate integrations.

3 Results

3.1 PEC Sample Preparation

Following the methods described in the previous section, a bulk polyelectrolyte complex composed of PSS and PDADMA with weight average molecular weights of 200 and 200-350 kg · mol^{-1}, respectively, was prepared. NMR measurements on the salt-free, dry PEC confirmed that the PEC was stoichiometric (see Electronic Supplementary Information†). Samples with salt and polymer concentrations well above the binodal were then prepared from this dried PEC, as illustrated in Figure 2(a). The targeted sample compositions primarily had salt concentrations above 20 wt% and polymer concentrations above 16 wt% because this is the regime in which phase separation was previously suggested to occur[44]. We note that these compositions are well above the normal binodal curve and, as such, should be in the single-phase regime. Photographs of representative samples obtained after equilibration are shown in Figure 2(b). As seen in this figure, phase separation was indeed observed in this composition range, and generally became more pronounced with increasing salt or increasing polymer concentration. At the lowest salt concentrations studied, the samples were clear and homogeneous. As the salt concentration increased, the samples became cloudy and then separated into two distinct phases, with an opaque, gel-like lower phase and a liquid-like upper phase that became increasingly clear and transparent with increasing salt concentration. Similar trends were observed with increasing polymer concentration, with the volume of the gel-like lower phase increasing as the polymer concentration increased. At the highest salt and polymer concentrations studied, the gel-like and liquid-like phases did not separate cleanly into distinct lower and upper phases, but were instead somewhat intermixed, likely because the relaxation dynamics were too slow for the gel-like phase to flow to the bottom of the tube. No significant changes to the appearance of the samples were noted over more than four weeks at room temperature, or in selected samples heated to 60 °C for more than one week. Finally, we note that the appearance and qualitative properties of the phases in this upper phase window (UPW) were different from those of phase-separated samples prepared below the binodal. Below the binodal, the polymer-rich lower phase was a translucent, viscous liquid, while in the UPW, the lower phase was an opaque gel. Interestingly, however, the upper phase was a relatively transparent, low-viscosity liquid in both regimes.

3.2 Phase Behavior

The phase behavior of the samples prepared in the UPW was quantified via TGA. Representative TGA traces of the upper and lower phases of a sample prepared in the normal binodal regime are shown in Fig. 3(a), while TGA traces of the upper and lower phases of a sample prepared in the UPW are shown in Fig. 3(b). The TGA traces for all samples exhibit a sharp mass loss at 100 °C, which is attributed to the evaporation of water from the sample. Mass loss between 100 and 600 °C is attributed to decomposition of the organic components of the sample (PSS and PDADMA), while the remaining mass at temperatures above 600 °C comes from the salt and any other inorganic residue from decomposition of the polymer. As seen in Fig. 3(a), only the lower/denser phase of the sample prepared below the binodal shows an appreciable drop between 100 and 600 °C, indicating that this phase is polymer-rich while the upper phase/supernatant is polymer

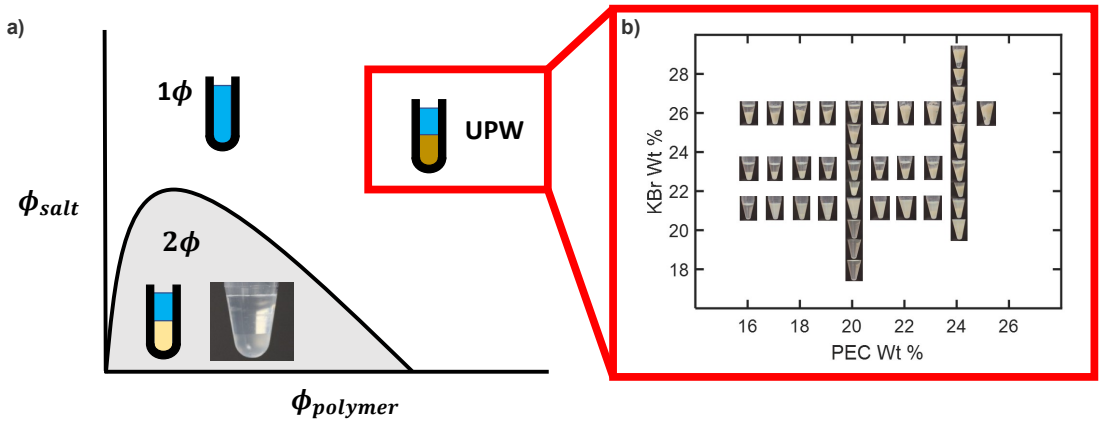

Fig. 2 (a) Schematic of a polyelectrolyte complex coacervate phase diagram illustrating both the binodal (solid line) and the sample compositions targeted in this work, and (b) representative images of samples prepared in the upper phase window at high salt and high polymer concentrations. Larger copies of all images shown in panel (b) are provided in the Electronic Supplementary Information†.

poor. The supernatant correspondingly has a higher mass loss attributed to water, while both phases have similar inorganic fractions. By contrast, as seen in Fig. 3(b), both the lower and upper phases of the sample prepared in the UPW show a significant mass loss in the 100-600 °C range, indicating that both phases have significant polymer content. The upper phase again has a higher water content, while the lower phase has a higher inorganic fraction. Interestingly, for samples prepared in the UPW, the mass loss corresponding to the polymer occurs at different temperatures in the upper and lower phases. The upper phase exhibits a sharp mass loss starting at about 350 °C, while the lower phase only begins losing mass around 500 °C. This is consistent with the possibility that the PSS and PDADMA, which have different combustion temperatures[45,46], partition into separate phases.

Full TGA traces for all samples are provided in the ESI, and their mass losses in the temperature ranges corresponding to their organic and inorganic components are summarized in Figure 4. We note that at first glance, this data suggests that the salt content of the phase-separated samples might be different in the UPW than in the normal binodal region. In particular, the amount of inorganic residue at high temperatures is higher in the polymer-rich lower phase of the UPW samples than in the polymer-poor upper phase, in stark contrast to the behavior observed for samples prepared under the binodal. However, in stoichiometrically-imbalanced samples the mass fraction of this residue does not necessarily reflect the true salt content of the material (see Electronic Supplementary Information), and correcting for this imbalance requires knowledge of the actual PSS/PDADMA stoichiometry in each sample.

3.3 Polymer Partitioning

To accurately determine the PSS/PDADMA ratios in each phase, we used the ^{1}H-NMR analysis described by Shamoun *et al.*[47] NMR spectra of the upper and lower phases of a representative sample are shown in Fig. 5. In this spectrum, the peaks between 5.5 and 9 ppm correspond to the 4 aromatic protons on PSS, while the peaks between 0 and 4.5 ppm correspond to the aliphatic protons on both PSS and PDADMA. For each phase, the fraction of all charged repeat units coming from PSS (x_{PSS}) in that phase was determined from the integrals of these peaks using

$$x_{PSS} = \frac{PSS}{PSS + PDADMA} = \frac{4I_{aromatic}}{4I_{aromatic} + (I_{aliphatic} - \frac{3}{4}I_{aromatic})} \quad (1)$$

where $I_{aromatic}$ is the integral of the aromatic protons and $I_{aliphatic}$ is the integral of the aliphatic protons, as described above. This analysis successfully reproduced the composition of a PEC prepared with a 1:1 mixture of PSS and PDADMA to within 1%, indicating that it provides accurate quantitative information about the sample composition. NMR spectra of all analyzed samples and the standard sample are provided in the Electronic Supplementary Information†.

The compositions of the samples extracted using NMR are summarized in Figures 6 and 7. As seen in these figures, at the lowest salt and polymer concentrations studied, the lower, denser phase contained almost exclusively PSS, while the PDADMA was primarily in the upper, less-dense phase. Increasing the PEC concentration while holding the KBr concentration constant (Fig. 6) and increasing the KBr concentration while holding the PEC concentration constant (Fig. 7) both brought the composition of the lower, denser phase back toward stoichiometric ($x_{PSS} = 0.5$). The trends in the composition of the upper, less-dense phase were less consistent; however, the volume of this phase also decreased dramatically with increasing PEC and KBr concentration, and the vast majority of the polymer was thus in the lower, denser phase. ATR-FTIR measurements yielded similar qualitative trends in the polymer partitioning as observed by NMR (see Electronic Supplementary Information†).

3.4 Phase Diagram of the UPW

Using the stoichiometry data obtained from NMR, the TGA data was corrected to obtain the true organic and inorganic mass frac-

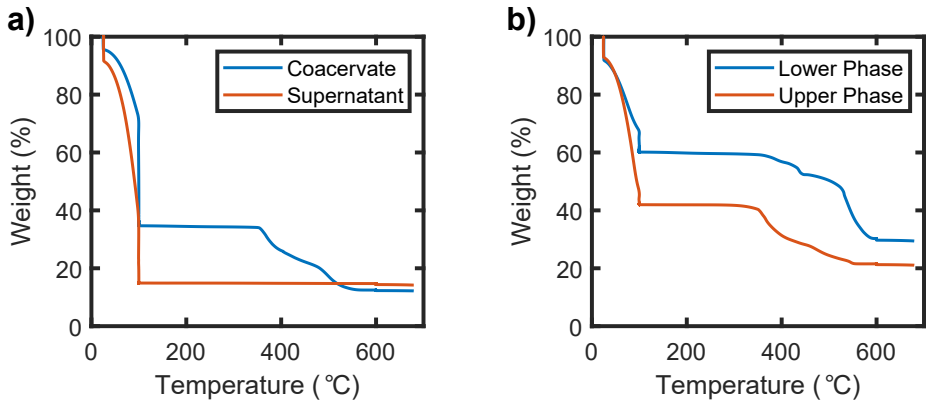

Fig. 3 TGA traces for (a) the coacervate and supernatant phases of a $PSS^-PDADMA^+$ sample prepared below the binodal and (b) the dense and dilute phase of a sample prepared at a composition far above the binodal. The sample prepared under the binodal had a target composition of 3% PEC and 14% KBr by mass. The sample prepared in the upper phase window had a target composition of 20% PEC and 21% KBr by mass. TGA traces of all other samples prepared in both the UPW and the normal binodal regime exhibited similar trends (see Electronic Supplementary Information†).

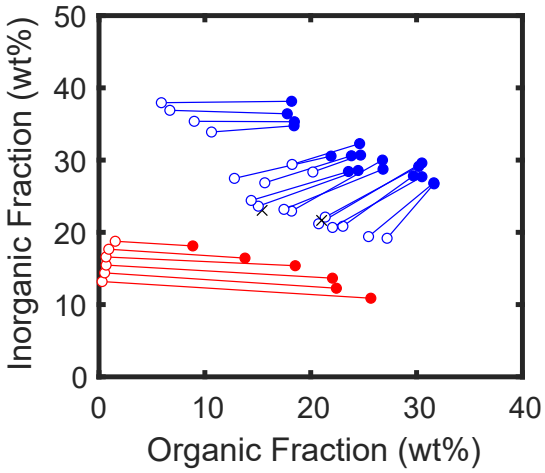

Fig. 4 Compositions of dense (filled circles) and dilute (open circles) layers of samples prepared at high salt and high polymer concentrations (blue) and samples prepared at low salt and polymer concentrations (red). Axes indicate the weight fraction of each phase attributed to organic components (polymer) and to inorganic components (including salt and any inorganic residues from polymer decomposition).

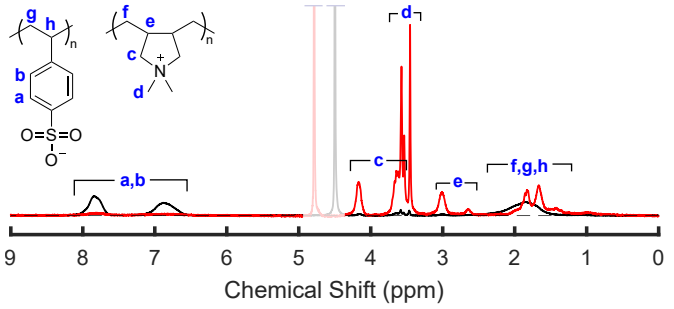

Fig. 5 Representative ^{1}H-NMR spectrum of the lower and upper phase of a sample prepared at high salt and high polymer concentrations (21% and 20% KBr and PEC, respectively). Samples were dried and dissolved in a 2.5 M solution of KBr in D_2O prior to measurement. Spectra are normalized to the same number of charged repeat units, and the greyed-out peak indicates the D_2O peak from the solvent. A detailed discussion of the NMR peak assignments is provided in the Electronic Supplementary Information†.

tions of each sample, as described in the Electronic Supplementary Information†. The corrected mass fractions of polymer, salt, and water in each sample were then converted to volume fractions using the bulk densities of each component (1.00 g · cm^{-3} for water, 1.27 g · cm^{-3} for PSS/PDADMA ion paired polymers[48,49], and 2.75 g · cm^{-3} for KBr; note that for the purposes of this analysis, the entire organic fraction of the sample was analyzed using the PSS/PDADMA density and the inorganic fraction was analyzed using the KBr density, even if the samples were not stoichiometric). The resulting phase diagram is shown in Figure 8. For samples prepared at low salt and polymer concentrations, shown in red, the points form the characteristic concave down binodal curve typically observed for polyelectrolyte complexes. The tie lines connecting the compositions in this regime are relatively flat, with only a slight negative slope, consistent with prior measurements and the athermal mixing observed in the PSS/PDADMA/KBr system[49]. For samples prepared at high salt and polymer concentrations, shown in blue, the points form a tilted, concave-up curve. In this regime, both phases contain a significant amount of polymer, in contrast to the phase behavior at lower salt concentrations. The tie lines connecting the dense and dilute phases also have a pronounced negative slope, indicating that the salt has a much stronger tendency to partition to the polymer poor phase than it does at lower salt concentrations.

3.5 Salting Out of Component Polymers

As noted in the introduction, segregative phase separation at high salt concentrations in systems containing poly(acrylic acid) is thought to be driven by PAA's unfavorable polymer-water interactions when protonated, which can drive salting out of PAA alone at high salt concentrations[42]. To determine whether simi-

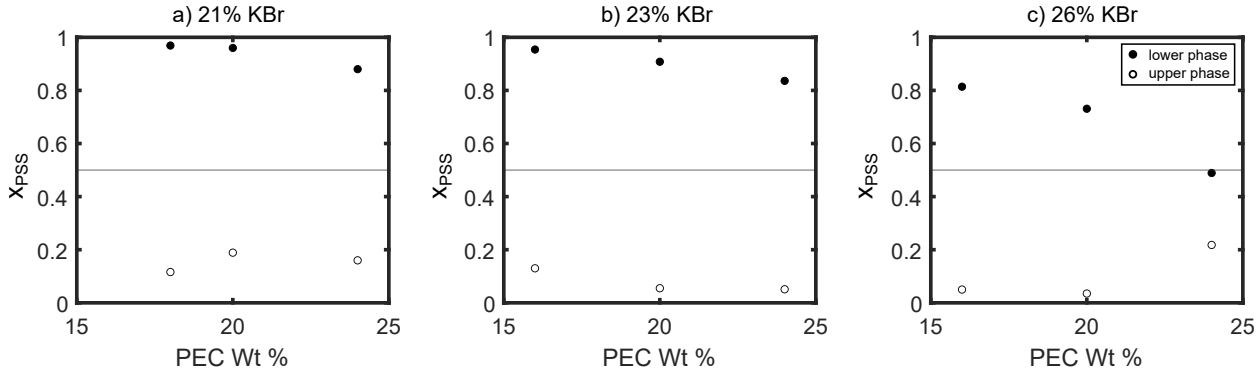

Fig. 6 Mole fraction of PSS in the dense (filled circles) and dilute (open circles) phases of samples prepared with (a) 21%, (b) 23%, and (c) 26% KBr by weight. The dashed line at $\chi_{PSS} = 0.5$ indicates the composition of a stoichiometrically-balanced mixture.

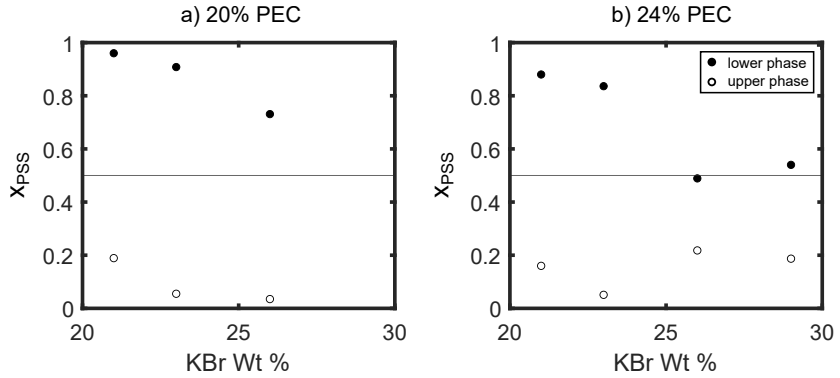

Fig. 7 Mole fraction of PSS in the dense (filled circles) and dilute (open circles) phases of samples prepared with (a) 20% and (b) 24% PEC by weight. The dashed line at $\chi_{PSS} = 0.5$ indicates the composition of a stoichiometrically-balanced mixture.

lar factors drive the segregative phase separation observed in the PSS/PDADMA system, independent samples of PSS and PDADMA were finally prepared at high salt concentrations. A polymer fraction of 15 wt% was chosen to approximate the concentration of each individual polyelectrolyte in the PEC samples. The compositions of the prepared samples, and their phase behaviors, are summarized in Table 1. As seen in this table, no phase separation was observed for any of the PDADMA samples. The PSS samples, however, phase separated at KBr fractions of 28% or higher. As in the rest of the UPW, the denser, lower phase was enriched in polymer while the less dense upper phase was enriched in salt. Interestingly, however, both the polymer-rich and polymer-poor phase of the samples prepared with both PSS and PDADMA had higher polymer content than the those of the samples prepared with PSS alone at similar salt concentrations, suggesting that interactions with PDADMA change the salting out behavior of the PSS, as described in more detail below.

4 Discussion

As noted in the introduction, the phase behavior of polyelectrolyte complexes and coacervates is typically well-described by a binodal curve with an upper critical salt concentration above which no phase separation occurs. Recently, however, studies have suggested that a second, segregatively phase-separated regime can occur at high salt concentrations in PECs prepared from weak, hydrophobic polyelectrolytes[40–42]. Here, we aimed to (1) determine whether a similar segregative phase separation occurs in strong polyelectrolyte systems, such as PSS/PDADMA; (2) characterize the phase behavior in this regime; and (3) provide detailed insight into the mechanism behind this phenomenon. As described above, these efforts were successful. As seen in Fig. 2, phase separation was indeed observed over a wide range of PSS/PDADMA and KBr concentrations at salt concentrations approximately 1 M above the binodal. Rigorous characterization by TGA, FTIR, and NMR showed that phase separation in this regime was indeed segregative, with PSS preferentially partitioning to the dense phase and PDADMA preferentially partitioning to the less dense supernatant. Interestingly, however, at the highest salt and polymer concentrations studied, both polymers were again found in the same polymer-dense phase. These observations provide useful new insights into the interplay between complexation and salting out of charged polymers, as discussed in more detail, below.

Segregative phase separation in neutral and like-charged polymer mixtures can occur when the individual polymer-solvent interactions are more favorable than the interactions between the different polymers[50–54]. Mixtures of oppositely-charged polymers typically undergo associative, rather than segregative, phase separation[1]. In polyelectrolyte mixtures containing poly(acrylic acid) (PAA) under conditions where the PAA is only partially

Table 1 Phase Behavior of PSS and PDADMA Solutions at High KBr Concentrations

Polymer	Prepared Composition		Phase[a]	Measured Composition		Corrected Composition[b]	
	PEC (wt%)	KBr (wt%)		Organic (wt%)	Inorganic (wt%)	ϕ_{pol}	ϕ_{KBr}
PSS	15	26	H	-	-	-	-
PSS	15	27	H	-	-	-	-
PSS	15	28	T	3.4	33.2	0.046	0.148
			B	15.7	32.4	0.211	0.126
PSS	15	29	T	2.1	35.4	0.029	0.162
			B	17.6	33.3	0.238	0.128
PSS	15	30	T	1.7	36.7	0.024	0.171
			B	13.8	35.1	0.189	0.144
PDADMA	15	26	H	-	-	-	-
PDADMA	15	27	H	-	-	-	-
PDADMA	15	28	H	-	-	-	-
PDADMA	15	29	H	-	-	-	-
PDADMA	15	30	H	-	-	-	-

[a] H = homogeneous, T = top/dilute layer, B = bottom/dense ;ayer; [b] Corrected according to the method described in the Electronic Supplementary Information[†]

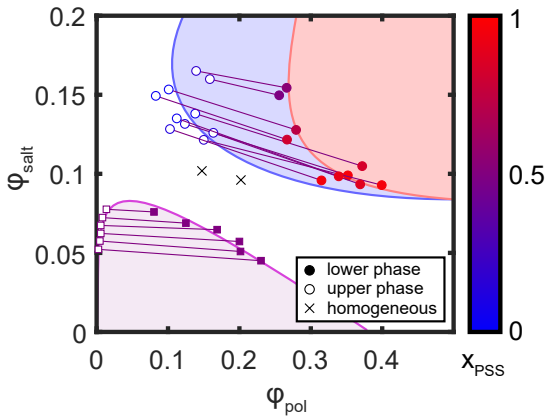

Fig. 8 Compositions of dense (filled circles) and dilute (open circles) layers of samples prepared at high salt and high polymer concentrations (upper right), plotted as a function of volume fraction of polymer (ϕ_{pol}) and volume fraction of salt (ϕ_{salt}). The color of each point indicates the mole fraction of PSS (x_{PSS}) in the sample. Compositions of the dense (coacervate) and dilute (supernatant) layers of samples prepared at lower salt and polymer concentrations (lower left) form the concave-down binodal curve typically observed in complex coacervate systems. Shaded regions indicate the approximate phase boundaries of the regions where PSS and PDADMA undergo associative phase separation (purple), PSS salts out (blue), and both PSS and PDADMA salt out (red).

charged[40,42], however, segregative phase behavior at high salt concentrations has been observed and attributed to increases in both the hydrophobicity and hydrogen bonding of PAA upon protonation[40]. As noted in the Introduction, Li et al. recently showed that this behavior can be predicted in theoretical models by increasing the Flory-Huggins interaction parameter for PAA-water interactions. Partial protonation of the PAA was suggested to be necessary to increase the polymer-water interaction parameter enough to drive re-entrant phase separation. However, Li et al.'s model does predict that when the polymer-water interaction parameter is high enough, re-entrant segregative phase separation may occur for mixtures of fully charged polyelectrolytes as well. Our work demonstrates that this can indeed occur: poly(styrene sulfonate) is a strong polyelectrolyte, with no pH dependent protonation behaviors, but segregative phase separation of PSS/PDADMA mixtures at high salt concentrations is clearly observed.

Strong polyelectrolytes are typically viewed as hydrophilic polymers because of their high charge content. From a chemical perspective, however, poly(styrene sulfonate) has substantial hydrophobic character[55], with both a nonpolar, aliphatic backbone and nonpolar aromatic rings on every repeat unit. Phase separation at high salt concentrations can thus be driven by favorable interactions between the polymer chains that dominate once the charge interactions are sufficiently screened, analogous to the salting-out effect observed in many biological systems[56,57]. As in protein solutions at high salt concentrations, salt-water interactions may also out-complete polymer-water interactions and effectively dehydrate the polymers, allowing hydrophobic interactions to drive aggregation[56]. Similar dehydration-driven coacervation has been observed in polyelectrolyte mixtures prepared in the presence of poly(ethylene glycol), which attracts water strongly enough to pull it away from the polyelectrolytes in the mixture[14]. This dehydration process effectively weakens the water-water and water-polyelectrolyte interactions and increases the polymer-water interaction parameter, in turn driving both the observed salting out of PSS from high-concentration KBr solutions and the segregative phase separation of PSS from PSS/PDADMA/KBr mixtures. We note, however, that in the UPW, samples typically contain only 5-10 water molecules per ionic site, in which limit mean field treatments and an average polymer-water interaction parameter may not accurately capture the physics of the system. The further preferential partitioning of water into the PDADMA-rich phase after phase separation is also consistent with a hydrophobicity-driven mechanism for this process, although the water content in the PSS-rich phase may also be affected by osmotic deswelling following phase separation.

Interestingly, while Li et al.'s model predicts that the dense

phase should almost exclusively contain the more hydrophobic polyelectrolyte (or, the polyelectrolyte with the highest polymer-water interaction parameter), we find that at the highest salt and polymer concentrations studied, the composition of the dense phase shifts back toward stoichiometric (Figs. 7 and 8). This suggests that at very high salt and polymer concentrations, both PSS and PDADMA salt out. Whether they salt out as individual polymers or as neutralized or partially-neutralized polyelectrolyte complexes, however, is not clear from the present data. We also note that comparison of the data in Table 1 with the phase diagram in Figure 8 (see also Electronic Supplementary Information†) suggests that at high salt concentrations, both the polymer-rich phase and the supernatant of samples prepared with PSS and PDADMA contain more polymer than the polymer-rich and polymer-poor phases of samples containing PSS alone. While this is expected for the supernatant (which, in PSS/PDADMA samples, must still contain PDADMA once the PSS salts out), it is somewhat less expected for the dense/polymer-rich phase (which would, in the absence of some type of PSS/PDADMA interaction, be expected to have the same polymer concentration as that samples prepared by salting out of PSS alone). This result thus suggests that the presence of PDADMA moderates the salting out of PSS, consistent with Li et al.'s prediction that the presence of both polyanion and polycation increases the polymer-water interaction parameter necessary to drive re-entrant phase separation[42].

A number of open questions remain about the re-entrant phase behavior observed in the upper phase window of the PSS/PDADMA system. First, the extent of hydrophobicity necessary to drive re-entrant, segregative phase behavior is not clear. While not the primary focus of our present work, we note that mixtures of PDADMA with poly(sulfopropyl acrylate) appear to exhibit similar phase behavior at high salt concentrations (see Electronic Supplementary Information†). Investigation of other, more hydrophilic strong polyanions, such as poly(2-acrylamido-2-methyl-1-propanesulfonate) or poly(vinyl sulfonate) may be useful for determining how much hydrophobic character is necessary to drive this behavior. Careful characterization of the viscoelasticity of the polymer-rich phase in these systems, if one is observed, may also help elucidate the role of hydrophobic interactions in driving the apparent gelation of the polymer-rich phase. Second, samples prepared at salt concentrations just above the critical salt concentration have been found to exhibit LCST behavior, phase separating upon moderate temperature increases[24]. While this behavior has been attributed to the temperature dependence of the dielectric constant of water, hydrophobic effects typically also increase in strength as temperature is increased[58]. Temperature dependent studies of the re-entrant, segregative phase separation observed at high salt concentrations should further elucidate the role of hydrophobic interactions in this phenomenon. Third, we note that the PSS and PDADMA samples used in this work were commercial samples which typically have very broad molecular weight distributions. Higher molecular weight polymers typically precipitate earlier than lower molecular weight polymers, and the phase behavior in Fig. 8 may be complicated by fractionation of the polymers. Studies on samples with narrower molecular weight distributions would be useful for determining the molecular weight dependence of re-entrant, segregative phase separation in these systems. Finally, at high polymer concentrations such as those used in our experiments, contributions from macromolecular crowding may be non-negligible[59–61]. Further experiments on polyelectrolyte mixtures at high concentrations with neutral crowders rather than salt may be useful for helping determine the relative contributions of salting out and crowding to the observed behavior. Together, these investigations will provide detailed insight into the polymer-water, polymer-salt, and salt-water interactions that govern the properties of polyelectrolyte complexes and coacervates, and inform understanding of these systems across a wide range of solution conditions.

5 Conclusion

Most studies of polyelectrolyte complexes and coacervates have focused on compositions under the binodal, with compositions above this boundary assumed to form only single-phase solutions. However, phase separation at high salt concentrations has been predicted for weak polyelectrolytes. Here, we showed that a second two-phase regime also emerges at high salt and high polymer concentrations in mixtures of strong polyelectrolytes. In a series of experiments on PSS/PDADMA samples, we observed phase separation in mixtures with polymer concentrations above approximately 16 wt% and salt concentrations above approximately 20 wt%. Critically, preparing samples by direct mixing of pre-formed PEC, KBr, and water enabled us to access samples with much higher concentrations of salt and polymer than achievable by conventional methods. As observed in weak polyelectrolyte systems, the phase-separated samples were not stoichiometric, even though the starting PEC was, suggesting that phase separation in this regime is segregative phase separation driven by salting out of the more hydrophobic polymer (PSS). The unexpectedly rich phase behavior observed in this upper phase window should provide exciting opportunities for furthering understanding of the chemistry and physics of these materials.

6 Data Availability

Supporting data for this manuscript (including all photographs and TGA, NMR, and FTIR traces) are provided in the Electronic Supplementary Information†. The corresponding raw data files are also available via the authors' institutional data repository, D-Scholarship@Pitt, at https://dx.doi.org/10.18117/9svg-9v48.

7 Conflicts of Interest

There are no conflicts of interest to declare.

8 Acknowledgments

This work was supported by a grant from the National Science Foundation (CHE-2203857). The authors thank Leanne Gilbertson for access to instrumentation used in this work.

References

1 C. E. Sing and S. L. Perry, *Soft Matter*, 2020, **16**, 2885–2914.
2 Y. Wang, S. Gao, W.-H. Ye, H. S. Yoon and Y.-Y. Yang, *Nature Materials*, 2006, **5**, 791–796.
3 S. K. Samal, M. Dash, S. V. Vlierberghe, D. L. Kaplan,

E. Chiellini, C. van Blitterswijk, L. Moroni and P. Dubruel, *Chemical Society Reviews*, 2012, **41**, 7147.
4 K. Osada, *Polymer Journal*, 2014, **46**, 469–475.
5 D. Sprouse and T. M. Reineke, *Biomacromolecules*, 2014, **15**, 2616–2628.
6 H. Shao, K. N. Bachus and R. J. Stewart, *Macromol. Biosci.*, 2009, **9**, 464–471.
7 W. Wei, Y. Tan, N. R. Martinez Rodriguez, J. Yu, J. N. Israelachvili and J. H. Waite, *Acta Biomater.*, 2014, **10**, 1663–1670.
8 H. J. Kim, B. Yang, T. Y. Park, S. Lim and H. J. Cha, *Soft Matter*, 2017, **13**, 7704–7716.
9 P. Schaaf and J. B. Schlenoff, *Adv. Mater.*, 2015, **27**, 2420–2432.
10 C. H. Porcel and J. B. Schlenoff, *Biomacromolecules*, 2009, **10**, 2968–2975.
11 X. Meng, S. L. Perry and J. D. Schiffman, *ACS Macro Letters*, 2017, **6**, 505–511.
12 M. T. Record, C. F. Anderson and T. M. Lohman, *Quarterly Reviews of Biophysics*, 1978, **11**, 103–178.
13 Z. Ou and M. Muthukumar, *The Journal of Chemical Physics*, 2006, **124**, 154902.
14 S. Park, R. Barnes, Y. Lin, B.-j. Jeon, S. Najafi, K. T. Delaney, G. H. Fredrickson, J.-E. Shea, D. S. Hwang and S. Han, *Communications Chemistry*, 2020, **3**, 83.
15 S. Chen and Z.-G. Wang, *Proceedings of the National Academy of Sciences*, 2022, **119**, e2209975119.
16 L. Li, A. M. Rumyantsev, S. Srivastava, S. Meng, J. J. de Pablo and M. V. Tirrell, *Macromolecules*, 2020, **54**, 105–114.
17 A. E. Neitzel, Y. N. Fang, B. Yu, A. M. Rumyantsev, J. J. de Pablo and M. V. Tirrell, *Macromolecules*, 2021, **54**, 6878–6890.
18 K. Sadman, Q. Wang, Y. Chen, B. Keshavarz, Z. Jiang and K. R. Shull, *Macromolecules*, 2017, **50**, 9417–9426.
19 Y. Luo, M. Gu, C. E. R. Edwards, M. T. Valentine and M. E. Helgeson, *Soft Matter*, 2022, **18**, 3063–3075.
20 A. B. Kayitmazer, A. F. Koksal and E. K. Iyilik, *Soft Matter*, 2015, **11**, 8605–8612.
21 J. Lou, S. Friedowitz, J. Qin and Y. Xia, *ACS Central Science*, 2019, **5**, 549–557.
22 J. Huang and J. E. Laaser, *ACS Macro Letters*, 2021, **10**, 1029–1034.
23 Z. Sui, J. A. Jaber and J. B. Schlenoff, *Macromolecules*, 2006, **39**, 8145–8152.
24 S. Ali, M. Bleuel and V. M. Prabhu, *ACS Macro Letters*, 2019, **8**, 289–293.
25 A. S. Ylitalo, C. Balzer, P. Zhang and Z.-G. Wang, *Macromolecules*, 2021, **54**, 11326–11337.
26 D. Priftis and M. Tirrell, *Soft Matter*, 2012, **8**, 9396–9405.
27 J. Fu, H. M. Fares and J. B. Schlenoff, *Macromolecules*, 2017, **50**, 1066–1074.
28 J. T. G. Overbeek and M. J. Voorn, *J. Cell. Comp. Physiol.*, 1957, **49**, 7–26.
29 K. T. Delaney and G. H. Fredrickson, *The Journal of Chemical Physics*, 2017, **146**, 224902.
30 M. Radhakrishna, K. Basu, Y. Liu, R. Shamsi, S. L. Perry and C. E. Sing, *Macromolecules*, 2017, **50**, 3030–3037.
31 T. K. Lytle and C. E. Sing, *Soft Matter*, 2017, **13**, 7001–7012.
32 A. M. Rumyantsev, E. B. Zhulina and O. V. Borisov, *Macromolecules*, 2018, **51**, 3788–3801.
33 M. Andreev, V. M. Prabhu, J. F. Douglas, M. Tirrell and J. J. de Pablo, *Macromolecules*, 2018, **51**, 6717–6723.
34 M. Rubinstein, Q. Liao and S. Panyukov, *Macromolecules*, 2018, **51**, 9572–9588.
35 M. Ghasemi, S. Friedowitz and R. G. Larson, *Macromolecules*, 2020, **53**, 6928–6945.
36 J. J. Madinya and C. E. Sing, *Macromolecules*, 2022, **55**, 2358–2373.
37 A. M. Rumyantsev, A. Johner, M. V. Tirrell and J. J. de Pablo, *Macromolecules*, 2022, **55**, 6260–6274.
38 C. E. Sing and J. Qin, *Macromolecules*, 2023, **56**, 5941–5963.
39 I. Konko, *Ph.D. thesis*, Universite de Strasbourg, 2015.
40 L. Li, S. Srivastava, S. Meng, J. M. Ting and M. V. Tirrell, *Macromolecules*, 2020, **53**, 7835–7844.
41 M. V. A. Queirós and W. Loh, *Polymers*, 2021, **13**, 2259.
42 H. Li, Y. Liu, F. Lan, M. Ghasemi and R. G. Larson, *Macromolecules*, 2023, **56**, 7909–7920.
43 P. Jha, P. Desai, J. Li and R. Larson, *Polymers*, 2014, **6**, 1414–1436.
44 F. J. Morin, M. L. Puppo and J. E. Laaser, *Soft Matter*, 2021, **17**, 1223–1231.
45 X. Lyu, B. Clark and A. M. Peterson, *J. Polym. Sci. B Polym. Phys.*, 2017, **55**, 684–691.
46 Q. Yao and C. A. Wilkie, *Polymer Degradation and Stability*, 1999, **66**, 379–384.
47 R. F. Shamoun, H. H. Hariri, R. A. Ghostine and J. B. Schlenoff, *Macromolecules*, 2012, **45**, 9759–9767.
48 H. M. Fares, Q. Wang, M. Yang and J. B. Schlenoff, *Macromolecules*, 2018, **52**, 610–619.
49 J. B. Schlenoff, M. Yang, Z. A. Digby and Q. Wang, *Macromolecules*, 2019, **52**, 9149–9159.
50 K. Bergfeldt, L. Piculell and P. Linse, *The Journal of Physical Chemistry*, 1996, **100**, 3680–3687.
51 M. W. Edelman, E. van der Linden, E. de Hoog and R. H. Tromp, *Biomacromolecules*, 2001, **2**, 1148–1154.
52 M. Vis, V. F. D. Peters, R. H. Tromp and B. H. Erné, *Langmuir*, 2014, **30**, 5755–5762.
53 I. K. Voets, A. de Keizer, P. de Waard, P. M. Frederik, P. H. H. Bomans, H. Schmalz, A. Walther, S. M. King, F. A. M. Leermakers and M. A. Cohen Stuart, *Angewandte Chemie International Edition*, 2006, **45**, 6673–6676.
54 M. Feric, N. Vaidya, T. S. Harmon, D. M. Mitrea, L. Zhu, T. M. Richardson, R. W. Kriwacki, R. V. Pappu and C. P. Brangwynne, *Cell*, 2016, **165**, 1686–1697.
55 B. A. Thurston, G. S. Grest and M. J. Stevens, *ACS Macro Letters*, 2022, **11**, 217–222.
56 T. Arakawa and S. N. Timasheff, *Biochemistry*, 1984, **23**,

5912–5923.
57 K. C. Duong-Ly and S. B. Gabelli, in *Methods in Enzymology*, Elsevier, 2014, pp. 85–94.
58 J. Schellman, *Biophysical Journal*, 1997, **73**, 2960–2964.
59 H.-X. Zhou, G. Rivas and A. P. Minton, *Annual Review of Biophysics*, 2008, **37**, 375–397.
60 Q. Bai, Q. Zhang, H. Jing, J. Chen and D. Liang, *The Journal of Physical Chemistry B*, 2020, **125**, 49–57.
61 B. Monterroso, W. Margolin, A. J. Boersma, G. Rivas, B. Poolman and S. Zorrilla, *Chemical Reviews*, 2024, **124**, 1899–1949.

Electronic Supplementary Information for:

Segregative Phase Separation of Strong Polyelectrolyte Complexes at High Salt and High Polymer Concentrations

Conner H. Chee, Rotem Benharush, Lexi R. Knight, and Jennifer E. Laaser*

S1 Supplemental Results

S1.1 Phase Behavior

Larger photographs of all phase-separated samples shown in Fig. 2(b) of the main text are included in Figure S1.

S1.2 Thermogravimetric Analysis

As discussed in the main text, the phase behavior of samples in both the normal binodal regime and the UPW was quantified by thermogravimetric analysis. Full TGA traces for samples prepared below the binodal are shown in Figure S2, and traces for samples prepared in the UPW are shown in Figure S3. As in the representative TGA traces shown in the main text, all samples prepared under the binodal exhibited distinct polymer-rich and polymer-poor phases, while samples prepared in the UPW had substantial salt and polymer content in both phases.

*Department of Chemistry, University of Pittsburgh, 219 Parkman Ave, Pittsburgh, PA, USA. E-mail: j.laaser@pitt.edu

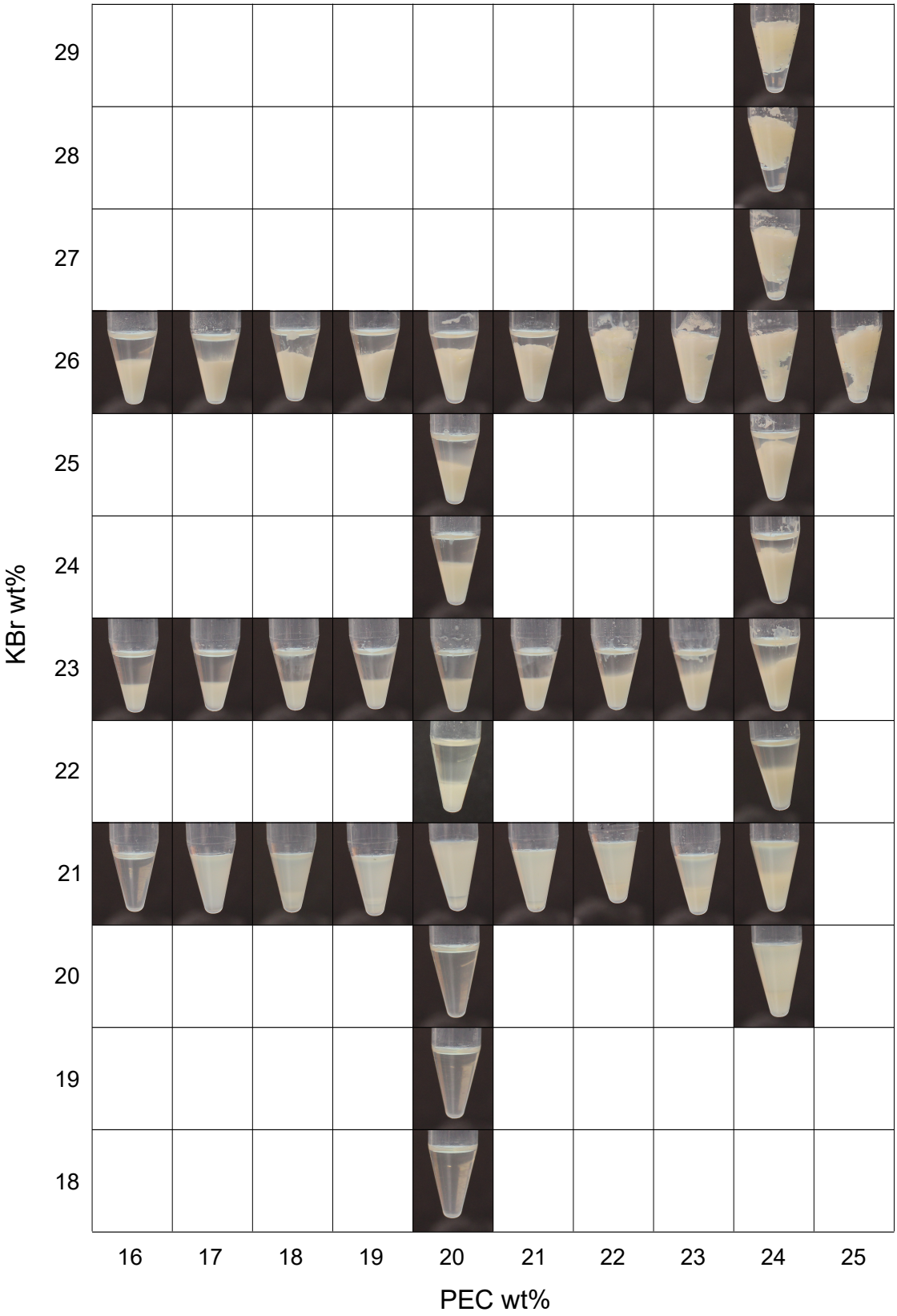

Figure S1. Photographs of samples prepared at high salt and polymer concentrations. Photos are labeled with the weight fractions of PEC and KBr at which each sample was prepared.

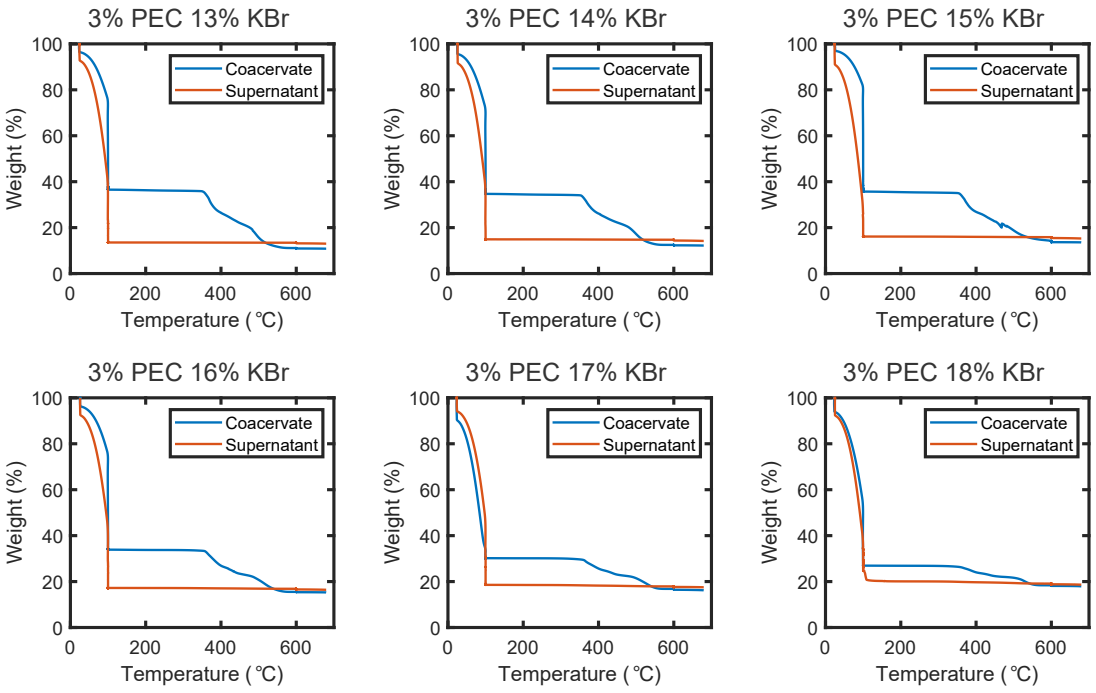

Figure S2. TGA traces of both phases of samples prepared under the binodal. The targeted weight fractions of PEC and KBr are listed above each panel.

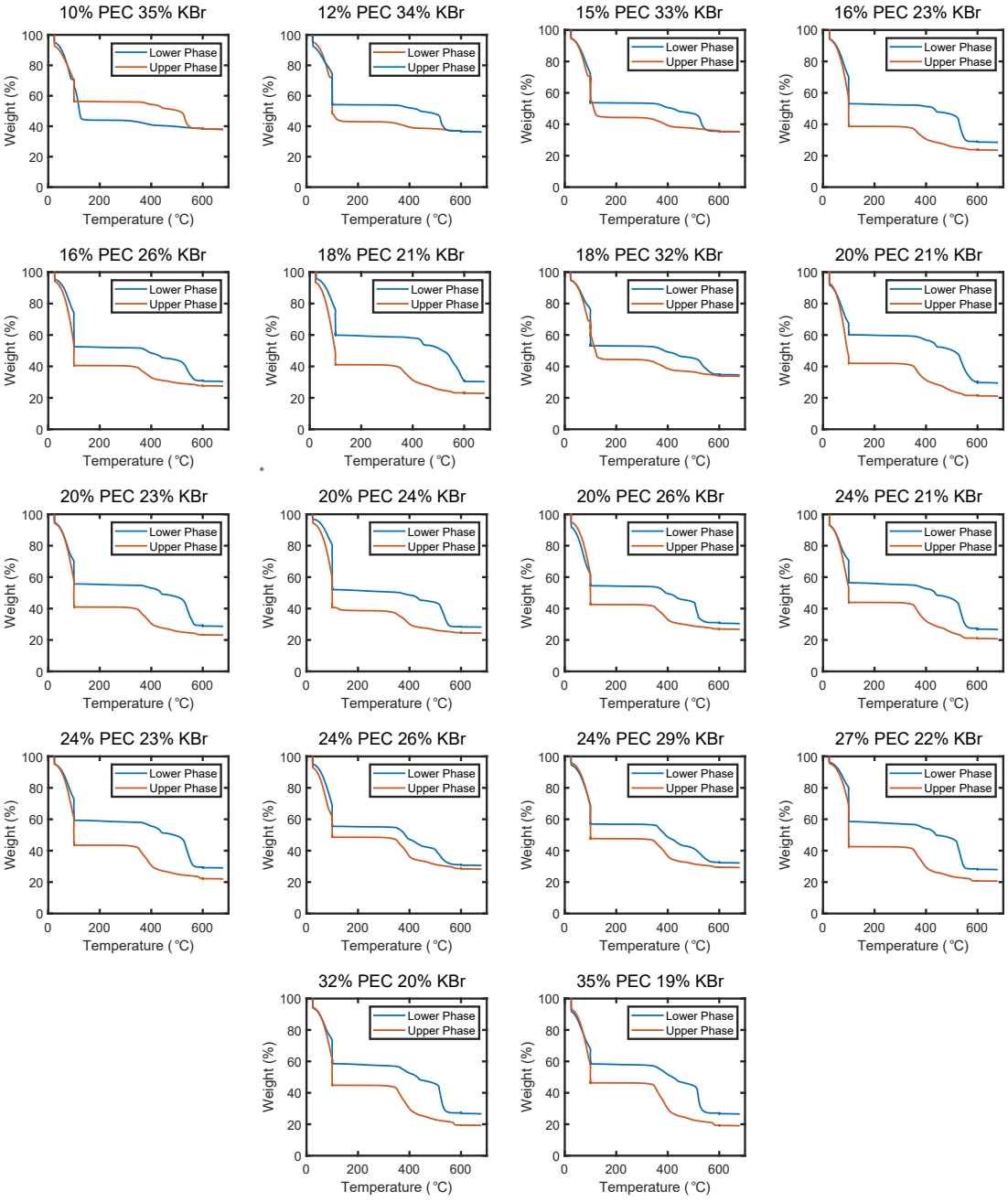

Figure S3. TGA traces of both phases of samples prepared in the UPW. The targeted weight fractions of PEC and KBr are listed above each panel.

TGA experiments were also carried out on samples of pure PSS^-K^+ (prepared by dialysis of PSS^-K^+ against KBr followed by milliQ water), pure $PDADMA^+Br^-$ (prepared by dialysis of $PDADMA^+Cl^-$ against KBr followed by milliQ water), and the salt-free PSS/PDADMA PEC used to prepare all samples. The resulting TGA traces are shown in Figure S4. As seen in this figure, the $PDADMA^+Br^-$ and PSS/PDADMA samples degraded completely by 600 °C under the conditions used for the TGA experiments. The PSS^-K^+, on the other hand, exhibited significant residue even at the highest temperatures (approximately 38% of the mass remained after the isotherm at 600 °C). This residual mass is consistent with degradation of PSS^-K^+ (chemical formula $C_8H_7O_3SK$, molecular weight 222.30 g/mol) to volatile products plus 0.5 eq. potassium sulfate (K_2SO_4, molecular weight 174.26 g/mol), although other inorganic byproducts (e.g. potassium sulfite) may also be present.

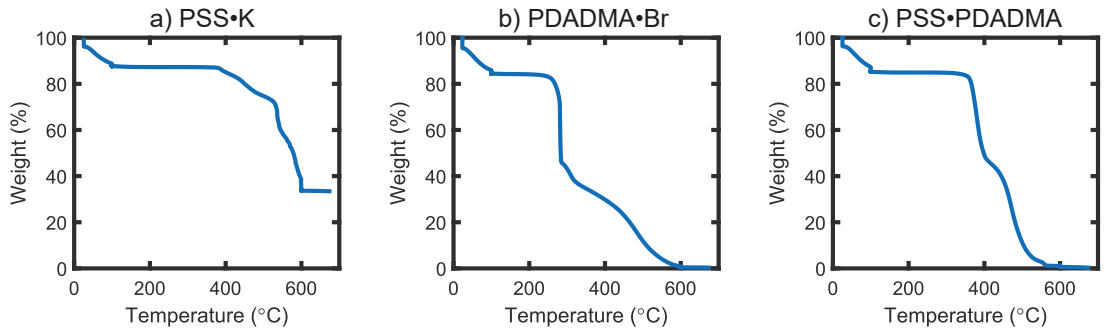

Figure S4. TGA traces of (a) PSS^-K^+, (b) $PDADMA^+Br^-$, and (c) salt-free PSS/PDADMA PEC. Samples were prepared from lyophilized, salt-free polymer samples; mass loss prior to 100 °C is attributed to loss of atmospheric water absorbed during sample preparation and transfer to the TGA pans.

S1.3 Nuclear Magnetic Resonance

Representative spectra of PSS, PDADMA, and a 1:1 stoichiometric PEC are shown in Fig. S5. In PSS, the protons from the aromatic rings appear between 6 and 8 ppm, and the protons from the backbone appear between 1 and 2 ppm. In PDADMA, the protons from the amine methyl groups appear between 3.3 and 3.8 ppm, the protons from the methylene units on the pyrrolidinium ring appear as two peaks of approximately equal intensity at 3.6 and 4.1 ppm, the protons from the

backbone methine appear as two peaks of unequal intensity at 2.6 and 2.9 ppm, and the protons from the backbone methylene units appear between 1.2 and 2 ppm. We note that the splitting of the pyrollidinium methylene and backbone methine peaks are often ignored in the literature, but are consistent with both the measured integrals and the expected splittings of protons on opposite faces of a substituted ring (for the pyrrolidinium methylenes) and the 6:1 cis:trans backbone stereochemistry previously reported for PDADMA (for the backbone methines).[1] The spectrum of the 1:1 PSS:PDADMA PEC, shown in Fig. S5(c), is essentially a linear combination of the individual PSS and PDADMA spectra, as expected. We note, however, that even though the number of PSS and PDADMA repeat units in the sample is the same, the peak intensity in the aliphatic region ($\delta < 4.5$ ppm) is significantly higher than the peak intensity in the aromatic region ($\delta \sim 6-8$ ppm) because of the large number of protons on each PDADMA repeat unit.

Spectra of all samples characterized in the UPW are shown in Figures S6-S8. In contrast to the spectrum of the stoichiometrically-balanced sample shown in Fig. S5(c), the ratios of the aromatic and aliphatic peaks vary widely, qualitatively indicating non-stoichiometric polymer partitioning.

As described in the main text, the stoichiometries of the individual phases were quantified from these spectra using

$$x_{PSS} = \frac{PSS}{PSS + PDADMA} = \frac{4I_{aromatic}}{4I_{aromatic} + (I_{aliphatic} - \frac{3}{4}I_{aromatic})} \tag{S1}$$

where $I_{aromatic}$ is the total intensity in the aromatic region (6-8 ppm) and I_{aliph} is the total intensity in the aliphatic region (1-4.5 ppm). This calculation, which is adapted from Shamoun et al.[2], is convenient because it does not require accounting for the splittings and overlaps of the peaks in the aliphatic region. However, with accurate assignment of the PDADMA spectrum, as described above, the mole fraction of PSS can also be calculated using

$$x_{PSS} = \frac{I_{aromatic}/4}{(I_{aromatic}/4 + I_{4.2}/2} \tag{S2}$$

where $I_{4.2}$ is the intensity of the peak at 4.2 ppm corresponding to half of the signal from the

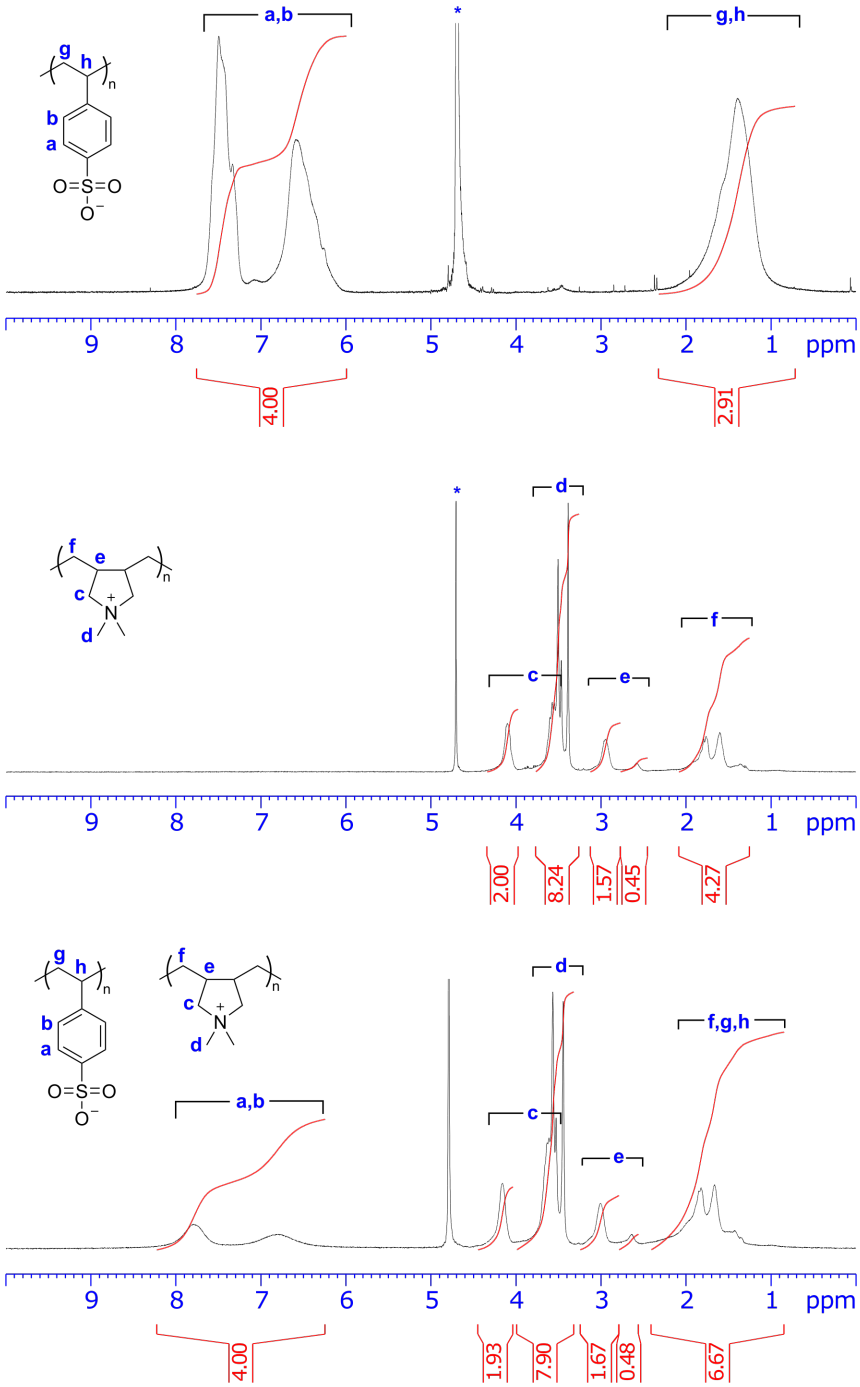

Figure S5. ^{1}H NMR spectra of (a) PSS, (b) PDADMA, and (c) a standard PEC composed of 1:1 PSS:PDADMA. In panel (c), analysis of the a,b and c peaks using equation S2 gives $x_{PSS} = 0.508$, while analysis of the total integrals of the aromatic and aliphatic regions using equation S1 gives $x_{PSS} = 0.506$.

pyrrolidinium methylenes. The integrals of the individual peaks used in these calculations, and the resulting values of x_{PSS}, are summarized in Table S1. As shown in this table, the x_{PSS} values

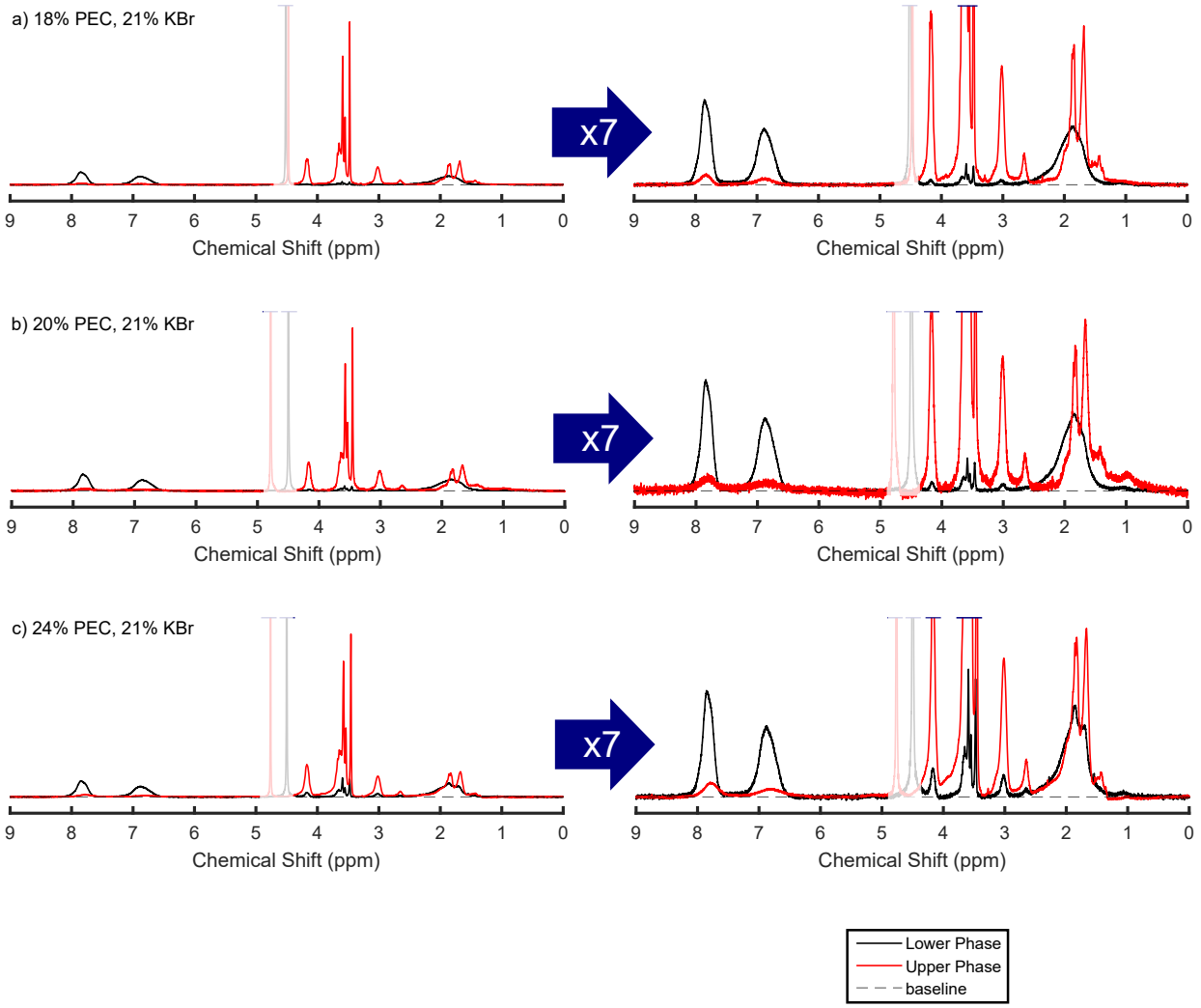

Figure S6. NMR spectra of both phases of samples prepared at 21 wt% KBr. The targeted weight fractions of PEC and KBr are listed above each figure. The left panel of each figure shows the full spectrum, while the right panel shows a 7x zoom. The baseline used for NMR integrals is indicated with a dashed line.

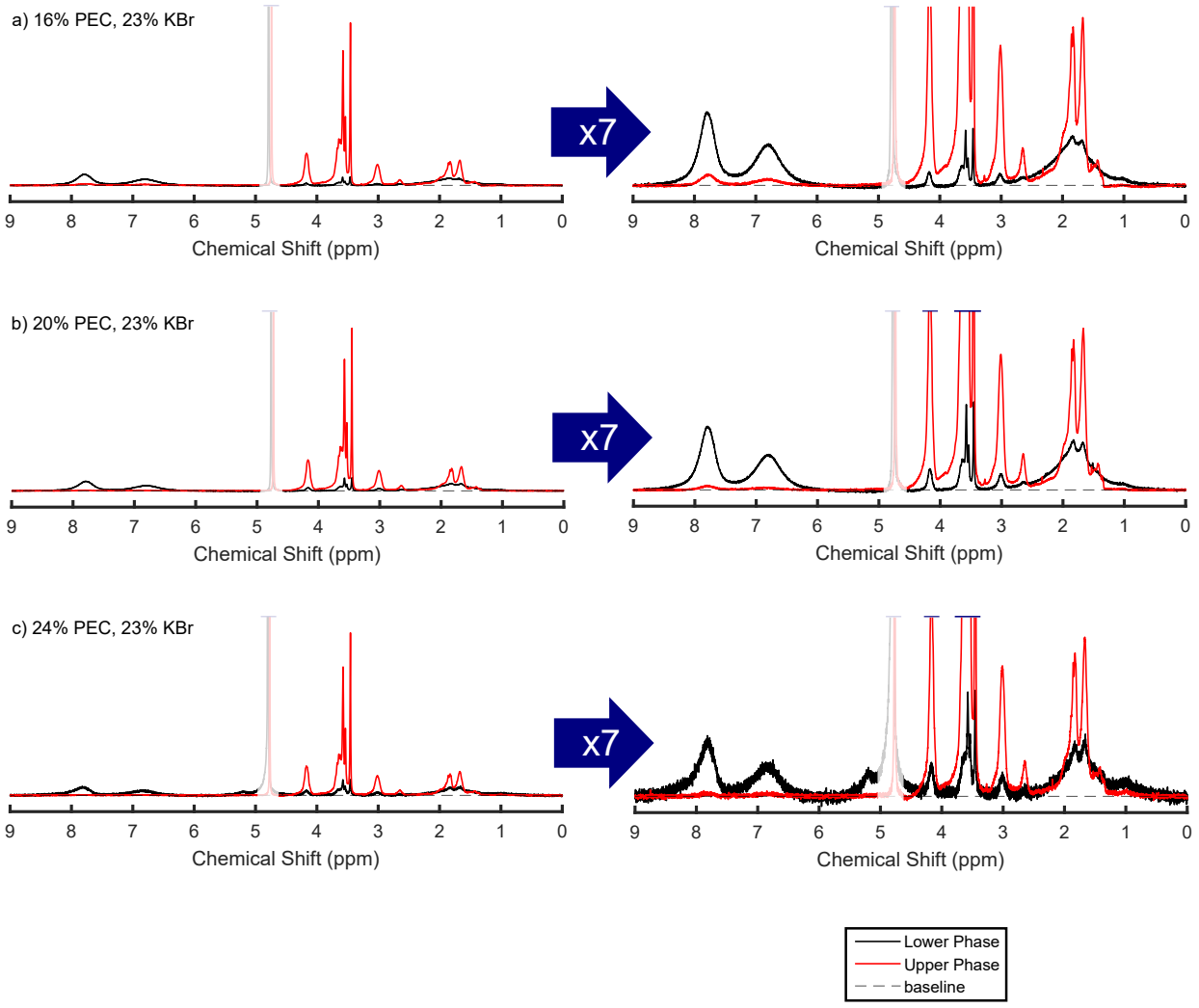

Figure S7. NMR spectra of both phases of samples prepared at 23 wt% KBr. The targeted weight fractions of PEC and KBr are listed above each figure. The left panel of each figure shows the full spectrum, while the right panel shows a 7x zoom. The baseline used for NMR integrals is indicated with a dashed line.

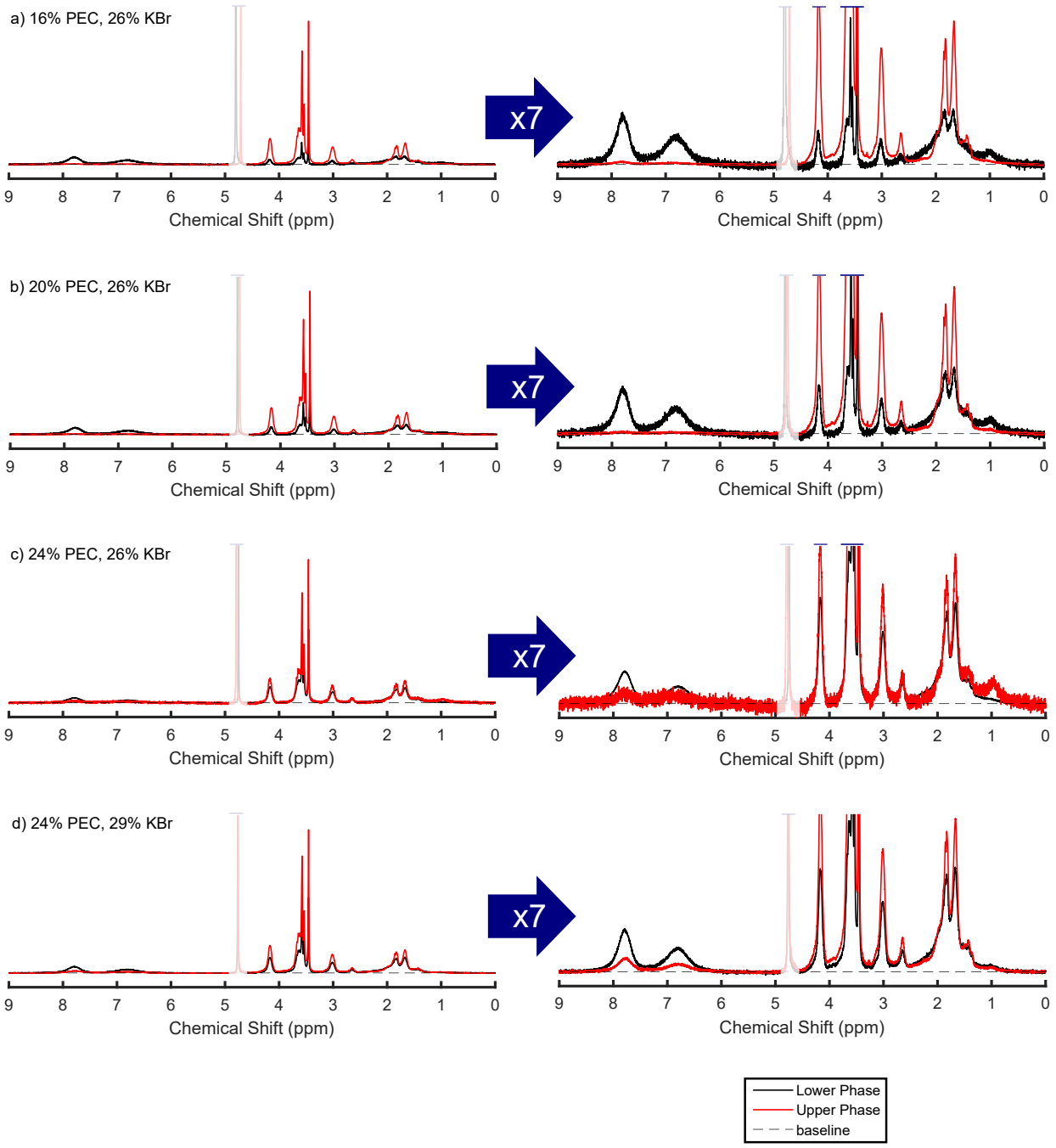

Figure S8. NMR spectra of both phases of samples prepared at 26 and 29 wt% KBr. The targeted weight fractions of PEC and KBr are listed above each figure. The left panel of each figure shows the full spectrum, while the right panel shows a 7x zoom. The baseline used for NMR integrals is indicated with a dashed line.

calculated by both methods agreed to within 5%. This variation is also consistent with the variation in x_{PSS} values between multiple independent measurements on the same sample, and 5% is thus used as the estimated error in the x_{PSS} values reported in this work.

Prepared Composition		Phase[a]	Integrals ($\times 10^{-3}$)					x_{PSS}	
PEC (wt%)	KBr (wt%)		6.4-8.2 ppm	4.0-4.3 ppm	3.3-3.8 ppm	2.5-3.2 ppm	0.8-2.5 ppm	Eq. S1	Eq. S2
18	21	L	135.7	1.6	7.4	4.3	106.2	0.969	0.977
		U	16.3	57.2	245.2	58.1	148.9	0.116	0.125
20	21	L	158.1	2.8	11.4	5.2	125.5	0.960	0.966
		U	5.9	10.7	49.0	12.3	33.9	0.189	0.216
24	21	L	105.5	6.0	27.3	8.0	95.3	0.880	0.898
		U	36.1	96.0	382.8	86.3	222.1	0.160	0.158
16	23	L	165.4	3.3	19.5	11.7	121.3	0.954	0.962
		U	28.1	94.4	378.9	87.5	217.7	0.130	0.130
20	23	L	179.2	8.1	39.7	16.1	143.5	0.908	0.917
		U	14.1	118.5	481.5	113.0	268.0	0.055	0.056
24	23	L	14.2	1.5	5.2	1.4	13.8	0.836	0.824
		U	4.4	38.4	161.0	37.9	93.2	0.051	0.054
16	26	L	21.2	1.7	9.1	2.5	22.0	0.814	0.862
		U	12.3	108.2	461.3	113.5	266.7	0.050	0.054
20	26	L	19.9	2.8	14.0	3.6	23.9	0.731	0.778
		U	5.7	73.1	312.1	76.1	178.8	0.035	0.038
24	26	L	141.7	64.4	276.0	71.7	237.9	0.489	0.506
		U	3.6	5.4	25.5	5.9	18.6	0.218	0.251
24	29	L	71.8	28.2	121.1	31.7	118.0	0.540	0.560
		U	31.5	65.0	271.0	66.2	172.3	0.187	0.196

[a] L = lower phase, U = upper phase

Table S1. Compositions of Phase-Separated Samples Obtained by ^{1}H-NMR

S1.4 Polymer Fraction

Plots of the polymer fraction in each sample, analogous the those for the mole fraction of PSS presented in Figures 6 and 7 in the main text, are presented in Figs. S9-S10.

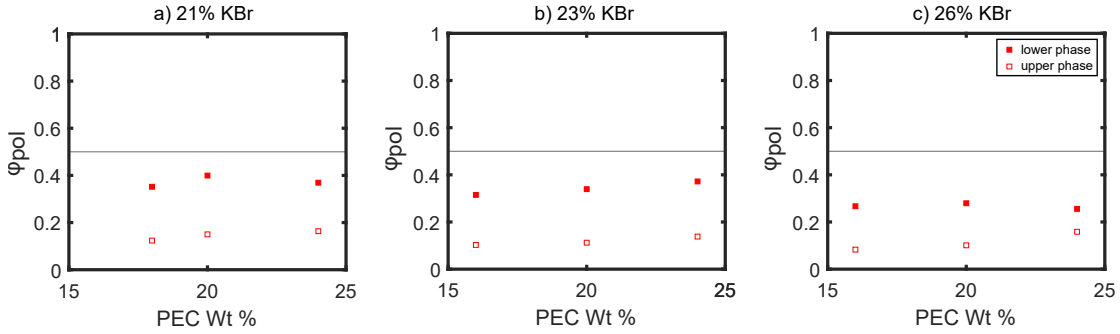

Figure S9. Volume fraction of polymer in the dense (filled squares) and dilute (open squares) phases of samples prepared with (a) 21%, (b) 23%, and (c) 26% KBr by weight.

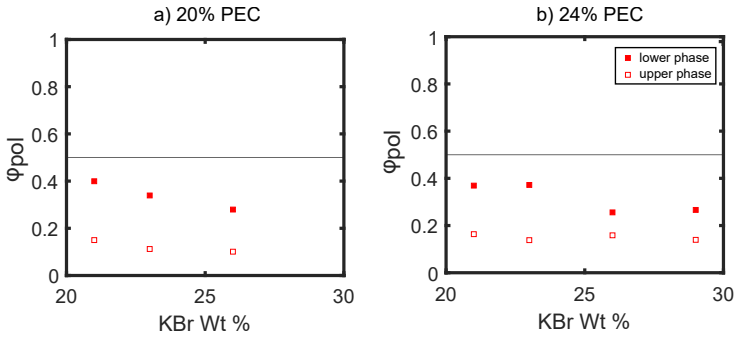

Figure S10. Volume fraction of polymer in the dense (filled squares) and dilute (open squares) phases of samples prepared with (a) 20% and (b) 24% PEC by weight.

S1.5 Infrared Spectroscopy

As noted in the main text, the TGA analysis suggested that PSS and PDADMA partition into different phases in the UPW. While ^{1}H NMR was used as the primary method for quantifying this partitioning, ATR-FTIR measurements were also performed to (1) provide further evidence for segregative phase separation and (2) determine whether there are are significant differences in the polymer hydration in these two phases. Representative IR spectra of the upper and lower phases

of a sample prepared in the UPW are shown in Figure S11. This spectrum exhibits a number of distinct features that are attributable to different molecular species in the sample. The peaks between 3700-2700 cm^{-1} and 1800-1600 cm^{-1} correspond to the stretching and bending modes of water, respectively. The peaks at 1450 and 1400 cm^{-1} correspond to the C-H stretching of the methyl group and C-N stretching modes of PDADMA, and the peaks at 1100 and 1000 cm^{-1} correspond to the C=C and S=O stretching modes of PSS. The shape of the peak corresponding to the water stretching mode between 3700 and 2700 cm^{-1} gives information about perturbation of the hydrogen-bonding network in the solvent. In both the upper and lower phases, this peak is narrower and somewhat blue-shifted compared to that of bulk water, indicating disruption of hydrogen bonds to accommodate the high polymer and salt concentrations[3]. The shape of this peak is similar for both the upper and lower phases, indicating that their hydration environments are comparable. As expected from the NMR measurements, however, the relative intensities of the peaks corresponding to PSS and PDADMA differed between the two phases. The peaks arising from PSS had a significantly stronger absorbance in the lower, polymer-rich phase, while the peaks arising from PDADMA had a slightly stronger absorbance in the upper phase. Spectra of other samples prepared in the UPW exhibited similar trends (Fig. S12). These results are qualitatively consistent with the partitioning observed by NMR, and provide further evidence for the occurence of segregative phase separation at high salt concentrations.

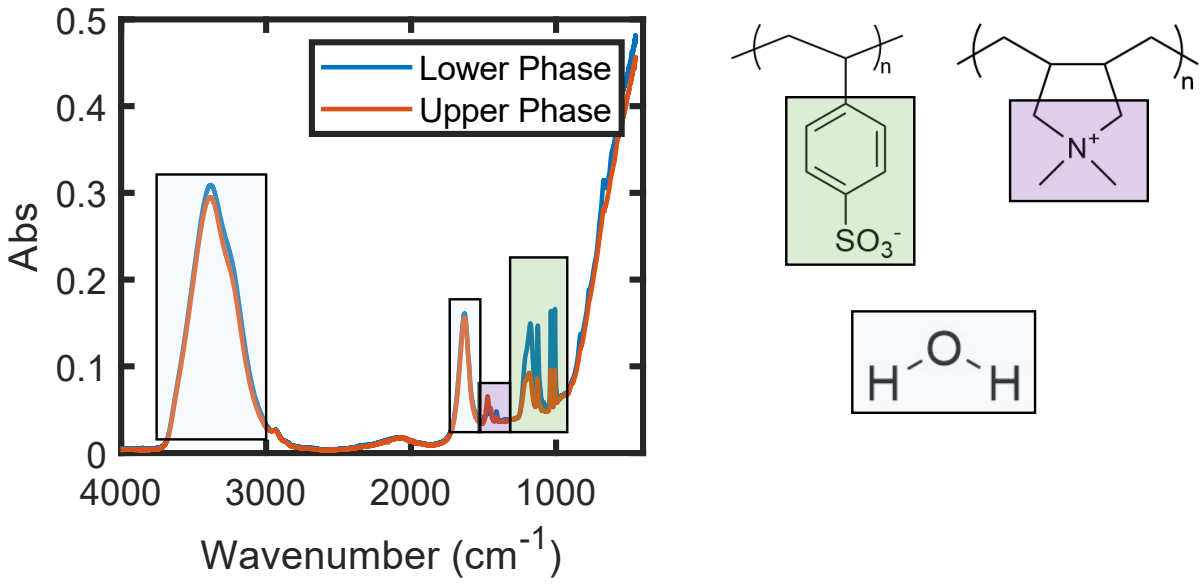

Figure S11. ATR-FTIR spectra of the lower and upper phases of a sample prepared at KBR and PEC concentrations of 21% and 20% KBr, respectively, with assignments of vibrational modes for each major peak in the spectrum.

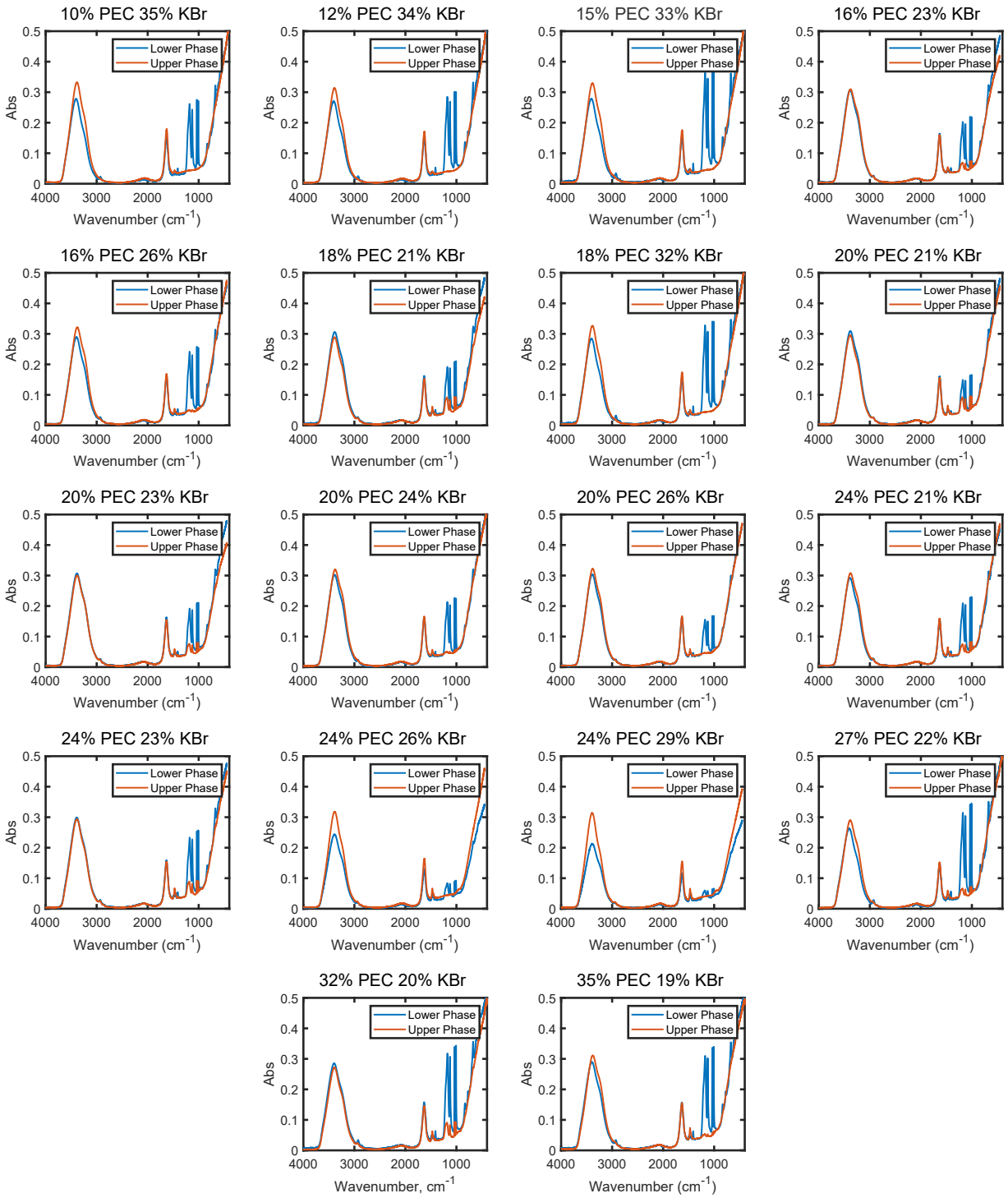

Figure S12. ATR-FTIR spectra of both phases of samples prepared in the UPW. The targeted weight fractions of PEC and KBr are listed above each figure.

S1.6 High-Salt Phase Behavior of PSPSA/PDADMA

As noted in the main text, a small number of experiments were also carried out on complexes of poly(sulfopropyl acrylate) (PSPA, $M_n \approx 200,000$ g/mol, Sigma-Aldrich) and poly(diallyldimethylammonium) (PDADMA, $M_w \approx 200,000 - 350,000$ g/mol, Sigma-Aldrich) in the presence of sodium chloride to determine whether phase separation in the UPW is unique to the PSS/PDADMA system or whether it is a more general phenomenon of strong polyelectrolytes. Samples were prepared using the same method as described for the $PSS^-PDADMA^+$ samples described in the main text. Photographs of samples prepared with PEC fractions of approximately 24 wt% and salt fractions between 14 and 23 wt% are shown in Figure S13. As seen in this figure, the PSPA/PDADMA system phase separated at salt concentrations above approximately 19 wt%, far above the binodal for this system. Interestingly, at the highest salt concentrations, a solid that appeared to be crystalline NaCl was also observed at the bottom of the dense phase, suggesting that NaCl actually becomes insoluble in the polymer solution at these high concentrations.

TGA traces for representative phase-separated samples prepared at both low and high salt concentrations are shown in Figure S14. As in the PSS/PDADMA system, samples prepared at low salt concentrations (underneath the conventional binodal) phase separated into a polymer-rich and a polymer-poor phase, while samples that phase separated at high salt concentrations contained significant polymer content in both phases. Finally, ATR-FTIR spectra of the upper and lower phases of the sample prepared at high salt concentrations, shown in Figure S15, indicated that the polymers also partitioned between the phases in a non-stoichiometric fashion, with the PSPA found primarily in the lower, denser-phase and the PDADMA found primarily in the upper, less-dense phase. Qualitatively, these trends match those observed in the PSS/PDADMA system, indicating that phase-separation in the UPW is a more general phenomenon of strong polyelectrolyte systems and is not restricted to aromatic polymers.

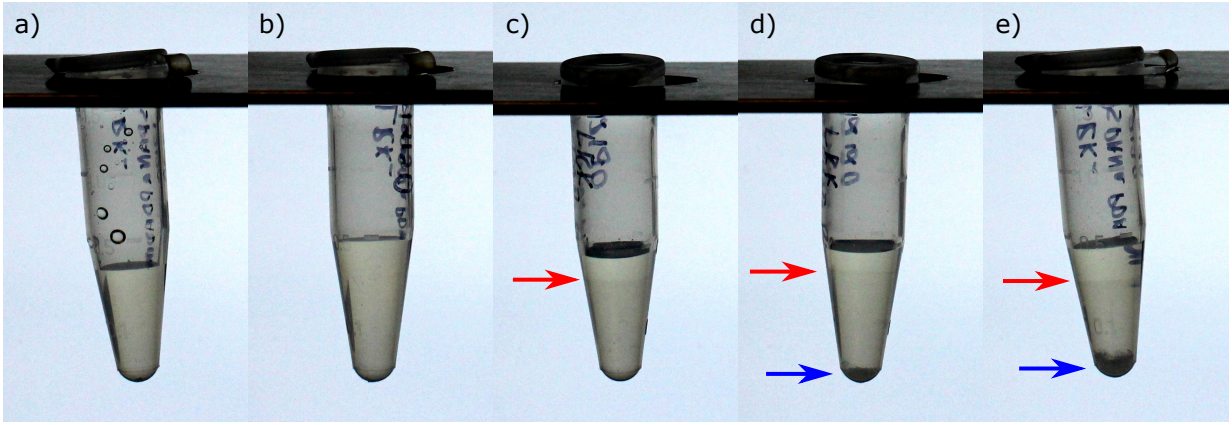

Figure S13. Photographs of PSS/PDADMA samples prepared with overall polymer fractions of 24 ± 1 wt% and NaCl fractions of (a) 14.4 wt%, (b) 16.4 wt%, (c) 19.3 wt%, (d) 21.3 wt%, and (e) 23.1 wt%. Red arrows indicate the boundary between the upper and lower liquid phases, while blue arrows indicate solid NaCl that did not dissolve at the highest salt concentrations.

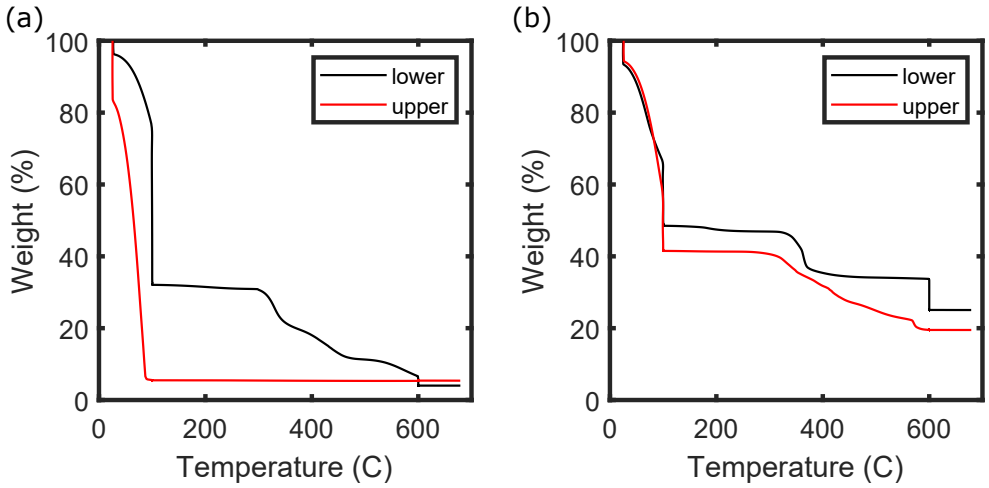

Figure S14. TGA traces of the upper and lower phases of PSPA/PDADMA samples prepared (a) at low salt and low polymer concentrations (0.1 M polymer and 0.8 M NaCl) and (b) high salt and high polymer concentrations (approx. 21.9 wt% polymer and 25.0 wt% NaCl).

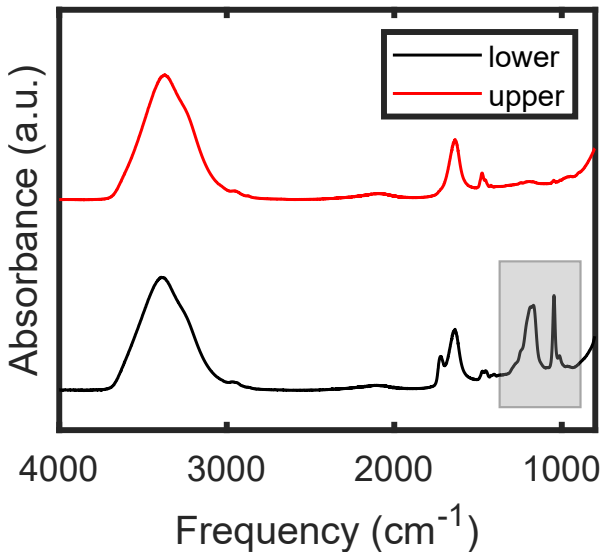

Figure S15. ATR-FTIR spectra of the upper and lower phases of a PSPA/PDADMA sample prepared at high salt and high polymer concentrations (approx. 21.9 wt% polymer and 25.0 wt% NaCl). The lower phase contains characteristic signatures of the sulfonate group (highlighted), while the upper phase does not.

S2 Supplemental Analysis

S2.1 Correction of TGA for Non-Stoichiometric Samples

As shown in Figure S4, samples of both $PDADMA^+Br^-$ and stoichiometric PDADMA/PSS complexes degrade completely before 600 °C in TGA experiments. Samples of PSS^-K^+, on the other hand, leave behind substantial residual mass at temperatures up to 700 °C, which we attribute to formation of non-volatile salts such as KSO_3 and K_2SO_4. As such, the mass loss between 100-600°C and the residual mass retained between 600-800 °C do *not* map directly onto the weight fractions of polymer and salt in the material, especially for samples containing excess PSS, and the TGA data for stoichiometrically-imbalanced samples must be corrected to obtain the true mass fractions of the organic and inorganic components prior to construction of the phase diagram.

This correction was performed as follows.

First, for each sample, we denote the *measured* mass loss at low temperatures (below 100 °C) as w_{low}, that at intermediate temperatures (100-600 °C) as w_{med}, and that at high temperatures

(>600 °C) as w_{high}. These values are *known*, or obtained directly from the TGA experiments. The *actual* mass fractions of water, PSS^-, $PDADMA^+$, K^+, and Br^- in the sample are denoted w_{H_2O}, w_{PSS}, w_{PDADMA}, w_K, and w_{Br}, respectively; these values are *unknown* and need to be determined from the analysis. Assuming that the mass loss below 100°C is attributable only to water, i.e.

$$w_{H_2O} = w_{low} \tag{S3}$$

this leaves four unknown values, requiring four constraint equations to uniquely determine their values.

For all samples, the first constraint arises from the requirement that the sample must be charge neutral. This constraint is expressed as

$$n_{PSS} + n_{Br} = n_{PDADMA} + n_K \tag{S4}$$

where n_{PSS}, n_{PDADMA}, n_{Br}, and n_K are the number of moles of PSS^- and $PDADMA^+$ repeat units and Br^- and K^+ ions, respectively. Written in terms of the weight fractions (which we interpret here as the mass of each species present in 1 g of sample), this constraint becomes

$$\frac{w_{PSS}}{m_{PSS}} + \frac{w_{Br}}{m_{Br}} = \frac{w_{PDADMA}}{m_{PDADMA}} + \frac{w_K}{m_K} \tag{S5}$$

where $m_{PSS} = 184.2$ g/mol, $m_{PDADMA} = 126.2$ g/mol, $m_{Br} = 79.9$ g/mol, and $m_K = 39.1$ g/mol are the molar masses of individual PSS^- and $PDADMA^+$ repeat units and Br^- and K^+ ions, respectively.

The second constraint for all samples is obtained from the PSS/PDADMA stoichiometry measured by NMR. The mole fraction of PSS in the organic component is given by

$$x_{PSS,PEC} = \frac{n_{PSS}}{n_{PSS} + n_{PDADMA}} \tag{S6}$$

or, in terms of weight fractions,

$$x_{PSS,PEC} = \frac{\frac{w_{PSS}}{m_{PSS}}}{\frac{w_{PSS}}{m_{PSS}} + \frac{w_{PDADMA}}{m_{PDADMA}}} \tag{S7}$$

The third and fourth constraints differ for samples with excess PDADMA and those with excess PSS.

For samples with excess PDADMA, since both stoichiometric $PSS^-PDADMA^+$ complexes and $PDADMA^+Br^-$ degrade completely below 600 °C, the mass loss between 100 and 600 °C corresponds to the mass of the stoichiometric portion of the $PSS^-PDADMA^+$ complex plus the mass of the stoichometric excess of $PDADMA^+Br^-$ (or, the mass of all of the the PSS^- and $PDADMA^+$, plus the mass of the Br^- ions associated with the excess $PDADMA^+$). This gives rise to the constraint

$$w_{med} = w_{PSS} + w_{PDADMA} + m_{Br}(n_{PDADMA} - n_{PSS}) \tag{S8}$$

$$= w_{PSS} + w_{PDADMA} + m_{Br}\left(\frac{w_{PDADMA}}{m_{PDADMA}} - \frac{w_{PSS}}{m_{PSS}}\right) \tag{S9}$$

The remaining mass above 600 °C then corresponds to the mass of the stoichiometric portion of the KBr (or, the total mass of K^+ and Br^- less the mass of the Br^- ions lost with the excess $PDADMA^+$), giving rise to the constraint

$$w_{high} = w_K + w_{Br} - m_{Br}(n_{PDADMA} - n_{PSS}) \tag{S10}$$

$$= w_K + w_{Br} - m_{Br}\left(\frac{w_{PDADMA}}{m_{PDADMA}} - \frac{w_{PSS}}{m_{PSS}}\right) \tag{S11}$$

Rearranging equations S5, S7, S9, and S11 yields the following system of four equations with four unknowns, which can be solved using appropriate numerical computing packages to obtain

the desired mass fractions of PSS^-, $PDADMA^+$, Br^-, and K^+ for each sample:

$$\begin{pmatrix} \frac{1}{m_{PSS}} & \frac{-1}{m_{PDADMA}} & \frac{-1}{m_K} & \frac{1}{m_{Br}} \\ \frac{x_{PSS,PEC}-1}{m_{PSS}} & \frac{x_{PSS,PEC}}{m_{PDADMA}} & 0 & 0 \\ 1-\frac{m_{Br}}{m_{PSS}} & 1+\frac{m_{Br}}{m_{PDADMA}} & 0 & 0 \\ \frac{m_{Br}}{m_{PSS}} & \frac{-m_{Br}}{m_{PDADMA}} & 1 & 1 \end{pmatrix} \begin{pmatrix} w_{PSS} \\ w_{PDADMA} \\ w_K \\ w_{Br} \end{pmatrix} = \begin{pmatrix} 0 \\ 0 \\ w_{med} \\ w_{high} \end{pmatrix} \tag{S12}$$

As shown in Fig. S4(a), samples containing only PSS^-K^+ lose approximately 60% of their non-water mass in the 100-600 °C range and the remaining 40% of their non-water mass in the 600-800 °C range. For mixed samples with excess PSS^-K^+, the mass loss in the 100-600°C range is thus the mass of the stoichiometric portion of the PEC plus 60% of the mass of the excess PSS^-K^+, while the mass loss in the 600-800 °C range is the mass of the stoichiometric portion of the KBr plus the remaining 40% of the mass of the excess PSS^-K^+. These constraints are expressed as

$$w_{med} = w_{PDADMA} + m_{PSS} n_{PDADMA} + f(m_{PSS}+m_K)(n_{PSS}-n_{PDADMA}) \tag{S13}$$

$$= w_{PDADMA} + m_{PSS}\frac{w_{PDADMA}}{m_{PDADMA}} + f(m_{PSS}+m_K)(\frac{w_{PSS}}{m_{PSS}} - \frac{w_{PDADMA}}{m_{PDADMA}}) \tag{S14}$$

and

$$w_{high} = w_{Br} + m_K n_{Br} + (1-f)(m_{PSS}+m_K)(n_{PSS}-n_{PDADMA}) \tag{S15}$$

$$= w_{Br} + m_K\frac{w_{Br}}{m_{Br}} + (1-f)(m_{PSS}+m_K)(\frac{w_{PSS}}{m_{PSS}} - \frac{w_{PDADMA}}{m_{PDADMA}}) \tag{S16}$$

where f is the fraction of the mass of excess PSS^-K^+ lost in the 100-600°C range ($f \approx 0.6$).

As in the excess PDADMA case, rearranging equations S5, S7, S14, and S16 yields the following system of four equations with four unknowns, which can be solved using appropriate numerical computing packages to obtain the desired mass fractions of PSS^-, $PDADMA^+$, Br^-, and K^+ for each sample:

$$\begin{pmatrix} \frac{1}{m_{PSS}} & \frac{-1}{m_{PDADMA}} & \frac{-1}{m_K} & \frac{1}{m_{Br}} \\ \frac{x_{PSS,PEC}-1}{m_{PSS}} & \frac{x_{PSS,PEC}}{m_{PDADMA}} & 0 & 0 \\ \frac{f(m_{PSS}+m_K)}{m_{PSS}} & 1+\frac{m_{PSS}-f(m_{PSS}+m_K)}{m_{PDADMA}} & 0 & 0 \\ \frac{(1-f)(m_{PSS}+m_K)}{m_{PSS}} & \frac{-(1-f)(m_{PSS}+m_K)}{m_{PDADMA}} & 0 & 1+\frac{m_K}{m_{Br}} \end{pmatrix} \begin{pmatrix} w_{PSS} \\ w_{PDADMA} \\ w_K \\ w_{Br} \end{pmatrix} = \begin{pmatrix} 0 \\ 0 \\ w_{med} \\ w_{high} \end{pmatrix} \tag{S17}$$

References

[1] J. E. Lancaster, L. Baccei and H. P. Panzer, *Journal of Polymer Science: Polymer Letters Edition*, 1976, **14**, 549–554.

[2] R. F. Shamoun, H. H. Hariri, R. A. Ghostine and J. B. Schlenoff, *Macromolecules*, 2012, **45**, 9759–9767.

[3] C. I. Eneh, M. J. Bolen, P. C. Suarez-Martinez, A. L. Bachmann, T. J. Zimudzi, M. A. Hickner, P. Batys, M. Sammalkorpi and J. L. Lutkenhaus, *Soft Matter*, 2020, **16**, 2291–2300.